Title
DETERMINATION OF THE KP-^tfV'vu, FORM FACTOR ?(q2) BY MUON POLARIZATION MEASUREMENTS

Author
Clark, A.R.

Publication Date
1976-08-01

Submitted to Physical Review D

LBL-4802 Rev.
Preprint

DETERMINATION OF THE $K_L^o \to \pi^- \mu^+ \nu_\mu$ FORM FACTOR $\xi(q^2)$ BY MUON POLARIZATION MEASUREMENTS

A. R. Clark, R. C. Field, W. R. Holley, Rolland P. Johnson, L. T. Kerth, R. C. Sah, and G. Shen

August 18, 1976

Prepared for the U. S. Energy Research and Development Administration under Contract W-7405-ENG-48

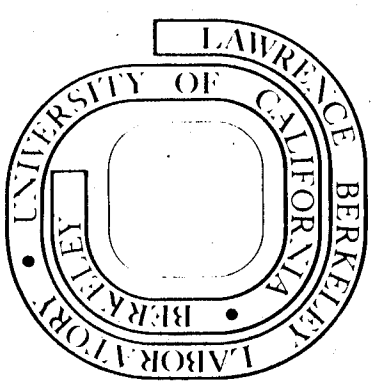

DISCLAIMER

LBL-4802
Revised

DETERMINATION OF THE $K_L^0 \to \pi^- \mu^+ \nu_\mu$ FORM FACTOR $\xi(q^2)$ BY MUON POLARIZATION MEASUREMENTS*

A.R. Clark, R.C. Field**, W.R. Holley, Rolland P. Johnson†
L.T. Kerth, R.C. Sah, and G. Shen †

Lawrence Berkeley Laboratory
University of California
Berkeley, California 97420

August 18, 1976

ABSTRACT

The polarization of the muon in the decay $K_L^0 \to \pi^- \mu^+ \nu_\mu$ ($K_{\mu 3}$) was measured as a function of q^2, the four-momentum transferred to the lepton pair, by using a precession polarimeter with a double-armed spectrometer at the Bevatron. A sample of 207,260 events collected with a vertical precession field was used to determine the $K_{\mu 3}$ form factor $\xi(q^2)$, assuming $\mathrm{Im}\xi(q^2) = 0.0$. If one parameterizes the q^2 dependence of ξ by $\xi(q^2) = \xi(0) + \Lambda q^2/m_\pi^2$, then $\xi(0) = 0.178 \pm 0.105 - 3.80\Lambda$. A sample of 55,604 events collected with a horizontal precession field was used to determine $\mathrm{Im}\xi(q^2)$. If one assumes that $\mathrm{Im}\xi(q^2)$ has no dependence on q^2, then $\mathrm{Im}\xi(0) = 0.35 \pm 0.30 + 0.21\ \mathrm{Re}\xi(0)$.

pendicular field was used to determine $\xi(q^2)$ under the assumption that $Im\xi(q^2) = 0.0$. The other orientation was used to determine $Im\xi(q^2)$.

The polarimeter and the rest of the apparatus, which are described in Section III, were designed to eliminate several potential sources of systematic error that existed in previous polarization experiments. More specifically, various earlier studies have relied on Monte Carlo simulations of acceptance and sometimes of background, an estimate of the polarimeter analyzing power, or significant background corrections. All of these have been avoided in this experiment.

The method of analysis is indicated in Section IV. The results are presented in Section V, along with a discussion of systematic effects.

II. THEORETICAL BACKGROUND

A. The $\xi(q^2)$ Form Factor

In the current-current model of the weak interactions, the matrix element for $K_{\mu 3}$ decay is

$$M = \frac{G}{\sqrt{2}} \langle \pi^- | J_\alpha^{HAD} | K^o_L \rangle \bar{\nu}_\mu \gamma_\alpha (1 + \gamma_5) \mu_\nu ,$$

if one ignores possible scalar and tensor couplings which have not been exhibited in any previous experiment.[3] One can represent this matrix element by a diagram (Fig. 1) in which all of the structure at the hadronic vertex is symbolized by a blob. The hadronic vertex is a function of three four-vectors, only two of which are independent by energy-momentum conservation. It is customary to choose $P_K - P_\pi$ and $P_K + P_\pi$ as a pair of basis vectors. Apart from the kaon and pion rest masses, there is only one independent scalar that can be formed from the basis vectors. It is customary to choose $q^2 = (P_K - P_\pi)^2$.

Since $\langle \pi^- | J_\alpha^{HAD} | K^o_L \rangle$ is a 4-vector representing the hadronic vertex, it must be expressible as a linear combination of the basis vectors, with coefficients that at most can depend on q^2. The traditional expression is

$$\langle \pi^- | J_\alpha^{HAD} | K^o_L \rangle = f_+(q^2)(P_K + P_\pi)_\alpha + f_-(q^2)(P_K - P_\pi)_\alpha . \qquad (II.1)$$

There is nothing fundamental about f_+ and f_-; any two independent functions related to f_+ and f_- will do. In particular, if we define

$$f_0(q^2) \equiv f_+(q^2) + \frac{q^2}{m_K^2 - m_\pi^2} f_-(q^2) , \qquad \text{(II.2)}$$

then $f_0(q^2)$ describes a $J^P = 0^+$ transition while $f_+(q^2)$ describes a $J^P = 1^-$ transition[4]. The precision Dalitz Plot study by Donaldson, et al.[1] suggests that the 1^- transition is dominated by the K* (890); and the 0^+ transition, to a less certain degree, is dominated by the enhancement in the κ (1200-1400) region.

For polarization experiments, it is convenient to work with yet another form factor, defined by

$$\xi(q^2) = f_-(q^2)/f_+(q^2).$$

From equation II.2 we see that

$$f_0(q^2)/f_+(q^2) = 1 + \frac{q^2}{m_K^2 - m_\pi^2} \xi(q^2),$$

so $\xi(q^2)$ determines the relative amplitude between a 0^+ and a 1^- transition.

There is thus a one-to-one relationship between the muon's polarization and the complex quantity $\xi(q^2)$ (c.f. Ref. 4). Cabibbo and Maksymowicz[5] have determined this relationship to be $\hat{S} = \vec{B}/|\vec{B}|$, where

$$\vec{B} = b_1(\xi)\left[(\vec{p}_\mu/m_\mu)\left(\vec{p}_\nu\cdot\vec{p}_\mu/(E_\mu+m_\mu)-E_\nu\right)+\vec{p}_\nu\right]$$
$$+\,b_2(\xi)\left[(\vec{p}_\mu/m_\mu)\;\vec{p}_K\cdot\vec{p}_\mu/(E_\mu+m_\mu)-E_K+\vec{p}_K\right]-(\mathrm{Im}\xi)\,\vec{d}\,,$$
$$b_1(\xi) = m_K^2 + m_\mu^2|b(q^2)|^2 + 2\left[\mathrm{Re}\;b(q^2)\right](q_\mu\cdot q_K),$$
$$b_2(\xi) = -2(q_\nu\cdot q_K) - \left[\mathrm{Re}\;b(q^2)\right](q^2-m_\mu^2),$$
$$b(q^2) = \frac{1}{2}\left[\xi(q^2)-1\right],$$
$$\vec{d} = E_K(\vec{p}_\mu\times\vec{p}_\pi)+E_\mu(\vec{p}_\pi\times\vec{p}_K)+E_\pi(\vec{p}_K\times\vec{p}_\mu)+\left[\vec{p}_\mu\cdot(\vec{p}_K\times\vec{p}_\pi)/(E_\mu+m_\mu)\right]\vec{p}_\mu\,,$$

(II.3)

and where the momentum vectors are defined in the laboratory frame.

Time reversal invariance specifies that $\xi(q^2)$ is real, which in turn implies that the polarization lies in the decay plane when viewed in the kaon's rest frame (see reference 5).

B. Kinematics

The $K^0_L \to \pi^-\mu^+\nu_\mu$ decay configuration has two degrees of freedom, aside from those related to rotations and translations. These are commonly chosen to be E^*_π and E^*_μ, the pion and muon total energies, respectively in the kaon's rest frame. Phase space is uniform in these two variables. The Dalitz plot is shown in Fig. 2a for $\mathrm{Im}\xi = 0.0$ and $\mathrm{Re}\xi = 0.0$. The Dalitz density is largest near the top and falls off roughly linearly as one moves

downward. Unfortunately, the greatest sensitivity of the polarization direction to variations in the ξ form factor occurs near the bottom of the Dalitz plot, for either $Re\xi(q^2)$ or $Im\xi(q^2)$. A measure of sensitivity is the angular change in polarization direction for a fixed change in $\xi(q^2)$. In the case of $Re\xi(q^2)$, the relevant angle is measured in the decay plane for a fixed change in $Re\xi(q^2)$. For $Im\xi(q^2)$, the relevant angle is the inclination of the polarization to the decay plane for a fixed change in $Im\xi(q^2)$. For statistical considerations, it is desirable to maximize the quantity

$$\text{polarization sensitivity} \times \sqrt{\text{population density}} .$$

For both $Re\xi$ and $Im\xi$, this quantity is maximized at approximately the same location in the Dalitz plot, indicated by an x in Fig. 2b. This compares with the actual phase space acceptance of this experiment shown in the same figure.

In addition to the above considerations, one must also consider the effects of the quadratic ambiguity. Since the apparatus does not measure the laboratory momentum of the K^o_L one can only determine that the K^o_L momentum is one of two possible solutions to a quadratic equation. A characteristic of the data is that the two solutions are usually located near each other on the Dalitz plot. Roughly speaking, the two configurations are mirror images reflected through a plane perpendicular to the beam line in the K^o_L rest frame. This reflection symmetry also applies to the muon's polarization and its sensitivity to $\xi(q^2)$. If one does not resolve the ambiguity, the resulting sensitivity becomes that of the expected polari-

zation vector; which is the vector sum of the two possible polarization vectors, weighted by their probabilities of being the correct solution. Since the two possible polarization vectors have mirrored sensitivities, they tend to cancel each other's effectiveness. Fortunately this cancellation is not complete. Due to the particular K^o_L momentum distribution of the events accepted in this experiment the solution corresponding to the lower K^o_L momentum is roughly twice as probable as the other solution. Thus about two thirds of the potential information is destroyed by the presence of the ambiguity.

C. Muon Decay Distribution

The muon polarization is measured using the direction of the positron emitted in the decay $\mu^+ \rightarrow e^+ \nu_e \bar{\nu}_\mu$.

In the V-A theory of the weak interactions, a muon at rest with polarization $\vec{s}$ will emit a positron whose momentum $\vec{p}$ has the distribution[6]

$$\frac{d^3N}{dp^3} \propto pE\left[(3 - 2x) + \frac{\vec{s}\cdot\vec{p}}{E} (1 - 2x) \right]$$

where $p = |\vec{p}|$, $E = (p^2 + m_e^2)^{\frac{1}{2}}$, $E_{max} = \frac{m_\mu^2 + m_e^2}{2m_\mu}$, and $x = E/E_{max}$.

In addition, the decay has a time distribution

$$\frac{dN}{dt} = \frac{1}{\tau} e^{-t/\tau} \quad .$$

Denoting the angle between $\vec{s}$ and $\vec{p}$ by θ_{sp}, the full positron distribution can be written in the form

$$\frac{d^4N}{dp^3dt} = e^{-t/\tau}\left[f(x) + g(x)\cos\theta_{sp}\right]$$

for some functions f and g of x.

If we imagine an infinitesimal positron detector located in the direction $\vec{p}$ from the muon, then d^4N/d^3pdt would be the probability density for a positron hitting the detector with momentum p at time t. If the detector has a detection efficiency $\eta(\vec{p}) = \eta(x,\Omega_p)$, the probability density for actually <u>detecting</u> a positron is

$$r(\vec{p},t) = \left(\frac{d^4N}{d^3pdt}\right)\eta(\vec{p}).$$

If the muon is in a magnetic field $\vec{B}$, its polarization vector will precess about $\vec{B}$ at the frequency $\omega_L = \frac{g_\mu e|\vec{B}|}{2m_\mu c}$:

$$\frac{d\vec{s}}{dt} = \omega_L\, \vec{s} \times \hat{B}\,.$$

Meanwhile, since the detector is fixed in the laboratory, $\vec{p}$ is time independent. The probability density for detecting a positron of momentum $\vec{p}$ at time t then takes the form

$$r(\vec{p},t) = e^{-t/\tau}\left[f'(\vec{p}) + g'(\vec{p})\cos(\omega_L t + \phi_s - \phi_p)\right]$$

where ϕ_s and ϕ_p are the initial azimuthal angles of $\vec{s}$ and $\vec{p}$ about $\vec{B}$, and f' and g' are some functions of $\vec{p}$.

III. EXPERIMENTAL APPARATUS

A. Introduction

The apparatus was a two-armed magnetic spectrometer (see Figure 3). K^0_L's traveling down the central axis decayed in a vacuum decay volume. The spectrometer arm containing the polarimeter was reserved for the acceptance of the secondary μ^+, while the other arm was used for the secondary π^- from $K^0_L \to \pi^- \mu^+ \nu_\mu$. The momentum of each of the charged secondaries was measured with a large aperture magnet bracketed by two upstream and three downstream magnetostrictive spark chambers. The muon stopped in the polarimeter and its magnetic moment precessed about a magnetic field until the muon decayed. The direction of the positron provided information on the azimuthal angle of the muon polarization vector at the time of decay.

Since the various kaon decay modes produce charged secondary particles-pions, muons, and electrons (or positrons), each spectrometer must identify a secondary from among these possibilities. To discriminate electrons from the slower pions and muons, each arm contained a threshold Cherenkov counter. Pions and muons were distinguished from each other by comparing their penetrations into the range device or polarimeter with their measured momenta.

An accepted event satisfies the following requirements: (1) no signal present from either Cherenkov counter, (2) the muon track segment

downstream of the magnet must be parallel to the beamline within 45 milliradians, (3) the muon must enter through the upstream end of the polarimeter, but not exit through the rear, (4) the muon and pion tracks must pass through the horizontal hodoscopes, and (5) the two particle tracks must be in time coincidence by passing through the pair of timing counters.

The event requirements ensured that both the pion and muon tracks downstream of the magnets were roughly parallel to the kaon beam. This meant that the spectrometer arms were approximate transverse momentum selectors. The magnets were set to select muons with an average transverse momentum of 0.176 GeV/c and pions with an average transverse momentum of 0.088 GeV/c. The low pion setting was intended to enhance the acceptance in the low pion energy region of the Dalitz plot.

To facilitate the description of the apparatus, a right-handed coordinate frame is used (see Fig. 3): (1) the +y axis is "up", (2) the +z axis lies along the beam center line, and (3) the +x axis is in the direction $\hat{y} \times \hat{z}$.

B. Beam

The neutral beam was produced from a copper target in the external proton beam of the Bevatron. The production angle was 3.7 degrees downward.

Beyond the target a steering magnet of the proton beam channel steered the primary beam away from the collimation system and swept charged secondaries horizontally. The remaining neutral beam then passed through a series of uranium collimators and vertical sweeping magnets. The aperture

was 2.4 degrees vertically and 1.0 degree horizontally.

The beam then passed through a decay region consisting of a vacuum box 5 meters in length. Since the decay region was more than 7.6 meters downstream of the target, the principal beam constituents were photons, neutrons, and K^0_L's. A quantity of 10^{12} protons hitting the target generated roughly 700,000 K^0_L's in the beam, with several hundred times as many neutrons and photons. The actual proton rate ranged from 4×10^{11} per second to 1.8×10^{12} per second.

After leaving the decay region, the beam passed though a helium-filled bag to a re-entrant beam dump downstream of the apparatus. Downstream of the magnets, the sides of the beam channel were lined with 15 cm of steel. The range device was shielded by 10 cm of steel, while the polarimeter was shielded by 10 cm of lead.

For the analysis of the data, the significant beam characteristics are the K^0_L momentum spectrum (equivalently, the momentum of the primary protons) and the presence or absence of high frequency time-dependent intensity structure. The stability of the proton momentum is characteristic of the Bevatron and is much better than our requirements. The Bevatron RF system was turned off while the data were being collected; thus there is no RF structure in the data.

C. Spectrometer Magnets

The spectrometer magnets were picture frame magnets with useful apertures approximately 66 cm high, 102 cm wide, and 178 cm long. They

were skewed from the beam axis in the horizontal plane by 6 degrees (see Fig. 3), making the average trajectory more symmetric with respect to the magnet midplane.

The magnet currents were recorded on the data tapes after each Bevatron spill. The muon spectrometer magnet was set to a line integral of 587 kilogauss-cm, corresponding to a change in transverse momentum of 0.176 GeV/c. The pion spectrometer arm was set to a line integral of 293 kilogauss-cm, corresponding to a change in transverse momentum of 0.088 GeV/c.

D. Spark Chambers

Each spectrometer arm contained two wire spark chambers upstream of the magnet, and three chambers on the downstream side. An additional chamber was placed between the carbon degrader and the polarimeter to study the multiple scattering of muons entering the polarimeter.

Each chamber provided spark coordinates in two orthogonal (x, y) directions. The middle downstream chamber was rotated in the chamber plane by 10 degrees in order to resolve multiple track ambiguities. The two upstream chambers were rotated about the y axis 12 degrees to make them more nearly normal to the average track (Fig. 3).

The sensitive area of the upstream chambers was 84 cm high and 100 cm wide. The sensitive area of the downstream chambers was 98 cm high and 109 cm wide. Each chamber consisted of two gaps, each made of two wire planes having orthogonal orientations. The four magnetostrictive wands gave two

horizontal and two vertical positions for each trajectory through the chamber. The 76 μm (0.003 in) aluminum wires were spaced every 1 millimeter. The gap was 9.5 mm and was filled with a gas mixture of 90% neon and 10% helium, 10% of which was bubbled through ethyl alcohol at room temperature. Details on the chamber construction and high-voltage supply are included in reference 7.

The spark and fiducial information was read out by magnetostrictive wires. The signals were amplified, differentiated, and detected with zero-crossing discriminators. The times of the resulting pulses were digitized in a system of scalers operating at 20 MHz (1 scaler count corresponds to 0.25 mm in the chamber).

In the two upstream chambers of the pion spectrometer, and the upstream chamber in the muon spectrometer, each wand was allotted six scalers. The remaining spectrometer chambers were allotted four scalers per wand and the polarimeter chamber, two.

The chambers could handle over 150 triggers per second. The actual trigger rate, however, was typically around 40 per second. Extraneous tracks in the spark chambers and hodoscopes were well within manageable limits. The multiplicity of a typical chamber gap was about 1.8 sparks per event, while each gap could support and record at least four sparks.

E. Cherenkov Counters

The Cherenkov counters were used to discriminate electrons from pions and muons. This was achieved by filling the counters with Freon 12 at atmospheric pressure. The Cherenkov light was collected by three 5-

inch RCA-4522 photomultiplier tubes, assisted by light-gathering cones[8] and a large concave reflector (see Fig. 4). Individual phototube signals were latched and recorded on the data tapes; an OR'd signal was used by the trigger logic.

In actual operation the beam-side phototube in the muon spectrometer was disconnected because of excessive noise. This did not seem to degrade the efficiency. Moreover, this Cherenkov counter was not critical to the final analysis since a positron entering the polarimeter does not produce a delayed signal.

Both Cherenkov counters were determined to be better than 99.6% efficient in a test beam[9]. The data from the present experiment indicate that the product of the efficiencies of the two Cherenkov counters was better than 95%. This is sufficient for our analysis, although there is no reason to doubt the earlier calibration of the Cherenkov counter in the pion spectrometer.

F. Scintillation Counters and Hodoscopes

Each Cherenkov counter was sandwiched, fore and aft, between two hodoscopes that consisted of vertical staves of scintillator. Each upstream hodoscope contained 28 staves 3.8 cm wide, 6.4 mm thick, and 97 cm high. Each downstream hodoscope contained 30 staves 3.96 cm wide, 1.27 cm thick, and 118 cm high. The photomultiplier tubes alternated between the top and the bottom of adjacent staves. These pairs of hodoscopes gave prompt angular

information for use in the trigger.

A hodoscope consisting of six horizontal scintillator staves was immediately in front of each upstream vertical hodoscope. The four center staves were 15 cm x 120 cm while the two outermost staves were 17.3 cm x 120 cm. The horizontal hodoscope was useful in restricting the area for each spark chamber that was searched by the track reconstruction program.

Just behind the downstream vertical hodoscopes was a set of two 122 cm x 122 cm timing counters (labeled T in Fig. 3) which, with their associated electronics, gave a coincident output to the trigger if the two secondaries penetrated the counters on their separate sides within about 10 nanoseconds (see reference 7).

G. Range Device

The pion spectrometer was terminated by a range-measuring device (Fig. 4). This device exploited the different penetrating abilities of pions and muons in order to discriminate between them. The front section of the range device was a one meter long graphite block which slowed muons and pions by energy loss, and attenuated pions by nuclear interactions. Two 19 mm-thick lead sheets, one upstream of the graphite and the other in the middle, converted electrons into showers which were absorbed by the graphite. The rear section was a multilayered sandwich of steel plates and 19 mm thick scintillators. Transverse dimensions were 122 cm x 122 cm. The thickness of steel separating consecutive scintillators ranged from 2.54 cm in the front to 10 cm in the rear. This unequal distribution of steel corresponded

roughly to a 7 percent increase in momentum for each additional scintillator. The momenta of muons stopping in the device ranged from 500 MeV/c to over 1600 MeV/c.

H. Polarimeter

The polarimeter (Fig. 5) had two important functions. It provided information relating to the direction of the positron from the muon decay. At the same time, it was a range-measuring device.

As a range device, it was preceded by a graphite and lead degrader identical to the one described in the preceding section. The polarimeter was a multilayered sandwich of 3.18 cm thick aluminum plates and 1.27 cm thick scintillator (1.91 cm for the two end counters) with transverse dimensions of 122 cm x 122 cm. There were thirty-one scintillation counters in all. The momenta of muons stopping in the polarimeter ranged from 600 MeV/c to 1070 MeV/c.

The sandwich was wrapped in two rectangular solenoids, each designed to produce a uniform magnetic field of 100 gauss. The polarimeter was entirely encased in a steel box with walls at least 4.6 cm thick to return the flux. (The top was slotted along the x direction to allow the light pipes through.) Depending on which solenoid was active, the magnetic field could be oriented along the x or y axes. The currents were periodically reversed to eliminate some systematic effects. The solenoid was made of hollow copper conductors, and water-cooled. Instead of a sloping pitch, each turn was wound in a plane except for a dogleg in one corner to enable the

current to pass from one turn to the next. The return path for the current included a straight section that ran along the vertical joint where the doglegs were. The vertical current components in the doglegs were thus cancelled by the current in the return path. The uniformity of the fields were measured to be within $\pm 0.5\%$ over the useful volume.

In order to obtain information on the muon's polarization, the parity violating property of muon decay that the higher momentum positrons are preferentially emitted in the direction of the muon polarization is used (see Section II-C). The average polarization will lie approximately in the horizontal laboratory plane since it is constrained to lie in the decay plane if $\mathrm{Im}\xi = 0.0$.

Because of the sandwich structure of the polarimeter, one can only determine if the positron was emitted in either the upstream ($z < 0$) or downstream ($z > 0$) hemisphere. With the magnetic field perpendicular to the z axis, the polarization of a muon stopped in the polarimeter rotates through an orientation approximately normal to the polarimeter plates. This occurrence is marked by an extremum in the upstream-downstream positron decay asymmetry. By knowing the time it takes to achieve this orientation, one can determine the azimuthal direction about the magnetic field of the original (unprecessed) polarization. This will be discussed in more detail in Section IV.

Limits on the accuracy of the phase determination due to construction imperfections were negligible in relation to the achieved statistical precision. The polarimeter plates were within 2 mrad of being normal to the laboratory z axis. The magnetic fields had deviations of $\lesssim \pm 5$ mrad from the x or y axes, which is acceptable since the resulting effect on the phase measurements has a cosine dependence.

The prime consideration in the polarimeter design is the precision in determining the angle of the muon's polarization. This precision increases with the decay asymmetry and the square root of the number of detected decays. Thicker plates result in fewer detected decays but an increased average asymmetry (see reference 6). This means that a compromise must be made in the amount of material that the positron is required to penetrate before it is registered in the data sample. In addition, thin scintillators are desirable to minimize the fraction of muons stopping in them, instead of in the aluminum plates. Muons stopping in scintillator are quickly depolarized.

With 1.27 cm scintillators, 3.18 cm aluminum plates, and the requirement of a two-scintillator coincidence to reduce background, the polarimeter had a measured analyzing power of 0.32, and an average positron detection efficiency calculated to be about 10%. The fraction of muons stopping in scintillator was calculated to be 16.3 percent, which was consistent with the data[10]. Of the two-scintillator coincidences, 23 percent came from muons stopping in scintillators, 59 percent came from muons stopping in

aluminum, and 18 percent arose from random backgrounds.

The nonferromagnetic property of the aluminum plates removes the possibility of local field distortions. It also leaves the strength of the external field essentially unchanged (the magnetic susceptibility is 16.5 x 10^{-6}),[11] although this is not important for the analysis. Since aluminum is a conductor, the polarization of a muon at rest in aluminum will behave as though it were in a vacuum[12,13].

In a typical event, a muon enters the polarimeter and comes to rest in one of the aluminum plates. The prompt scintillation counter signals indicate in which plate the muon has stopped. At the same time, the event trigger opens a gate that allows thirty scalers to count pulses from a 50 Megahertz crystal oscillator. The frequency never varied by more than 20 Hertz over the course of the experiment. Each scaler is associated with a different pair of adjacent counters. If a coincidence occurs in two adjacent counters after the prompt signal, the associated scaler is stopped. Ideally, the pair of counters involved is either immediately upstream or downstream of the aluminum plate that contained the stopped muon. In that case, the delayed coincidence is assumed to be due to the emitted positron passing through the two counters. The scaler value gives the muon's lifetime, and the location of the counter pair relative to the muon's stopping point determines if the positron was emitted into the upstream or downstream hemisphere. Other counter pairs away from the muon stopping point can be examined to study backgrounds.

Figure 6 indicates the various delayed-signal configurations relative to the muon stopping point and their interpretations. Note that muons stopping in scintillator and decaying downstream are distinguished, and are thus eliminated from the data sample. Muons stopping in scintillator and decaying upstream are indistinguishable from upstream decays from muons stopping in the next aluminum plate. Such muons are largely depolarized, so their observed effect is to reduce the analyzing power for upstream decays to 0.28. As shown in Section IV below, this does not bias the analysis.

I. Trigger

The event trigger maximized the acceptance of $K_{\mu 3}$ events with the muon stopping in the polarimeter and also accepted other kaon decay modes, as the trigger rate permitted, in order to examine several systematic effects of the apparatus. The trigger was generated by the coincidence of signals from the pair of timing counters, the horizontal hodoscopes, the pair of vertical hodoscopes in the muon spectrometer, and the first two polarimeter counters, provided there were no signals from the Cherenkov counter in the muon spectrometer or from the next-to-the-last polarimeter counter. The muon must stop at least two counters from either end due to the two-scintillator requirement on the muon decay. The timing of the trigger pulse was determined by the signal from the polarimeter's upstream counters. The trigger signal fired the spark chambers, strobed the

prompt data from the various counters into latches and started a 6.4 μsec gate (~3 muon lifetimes) which enabled the muon-lifetime scalers.

The pair of vertical hodoscopes in the muon spectrometer provided an approximate, but prompt, measure of the horizontal track angle. Each of the twenty-eight staves in the upstream hodoscope was tied by a coincidence matrix to the six downstream staves most directly behind it. The matrix output was part of the event trigger. An output from the matrix indicated that a track was within 45 milliradians of being parallel to the beamline -- independent of its transverse position. The apparatus thus selected muons within a restricted range of transverse momenta.

The coincidence of the first two upstream polarimeter counters ensured that the muon candidate had penetrated at least two counters into the polarimeter. The veto provision from the next-to-the-last polarimeter counter ensured that the muon candidate did not exit through the downstream end of the polarimeter. The Cherenkov counter veto on the muon spectrometer arm suppressed triggers from $K^0_L \rightarrow \pi^- e^+ \nu_e$ decays.

J. Event Readout

Events were read out by a standard Lawrence Berkeley Laboratory (LBL) NIDBUS[14] system into a PDP-9 minicomputer. A memory buffer stored information from seven events, each packed into 240 eighteen-bit words. When the buffer was filled, it was rolled out to a disk, allowing the PDP-9 to continue collecting data. Between Bevatron spills, the buffers stored on the disk were written onto magnetic tape.

The information stored on tape included latches for all scintillation counters including those in the polarimeter and range device, latches for both Cherenkov counters, spark chamber information, and the contents of the polarimeter scalers. Other information recorded at the end of each beam spill included the current readings for the two spectrometer magnets and the polarimeter magnet, and the values from several diagnostic scalers.

IV. METHOD OF ANALYSIS

A. Introduction

Part H of Section III outlined how the polarimeter measured the polarization direction projected on the laboratory plane perpendicular to the precessing field. In muon decay, the higher momentum positrons are preferentially emitted in the direction of the polarization. As the polarization vector precesses about the polarimeter's magnetic field, the probability that the positron will be emitted into either the upstream or downstream hemisphere will rise and fall with it. The resulting positron time distribution for either hemisphere will be shown to satisfy the parametric form

$$R(t) = Ne^{-t/\tau}\left[1 + \alpha\cos(\omega t + \phi)\right]$$

The initial phase ϕ of the time distribution corresponds to the angle between the z axis and the projection of the original polarization vector in the plane perpendicular to the magnetic field.

Since the data actually consist of a collection of muons with various polarizations stopping in different regions of the polarimeter, ϕ will equal the projected angle of the vector sum of the polarizations over the subset of events displaying a muon decay in the polarimeter.

The quadratic ambiguity mentioned in Part B of Section I adds one final complication; even if $\xi(q^2)$ were known perfectly, the polarization of any given event cannot be uniquely predicted. Two possible solutions exist in general. However, since it is possible to calculate the probability that the correct solution is one or the other, the expected polarization can be computed by adding the two solutions, each weighted by its probability. So "polarization" is replaced by "expected polarization" in the preceding interpretation of ϕ.

To determine $\xi(q^2)$, the approach is to make several guesses at the value of $\xi(q^2)$ and, using the Cabibbo-Maksymowicz formula, compute the corresponding expected polarizations for each event. Of course, the guesses of $\xi(q^2)$ are systematically chosen to allow interpolating between guesses. The vector sums of these expected polarizations over the data sample will be the expected polarization of the data sample as a function of $\xi(q^2)$. Simultaneously, the positron time distributions for the upstream and downstream hemispheres are accumulated. This results in a predicted value of ϕ for each guess of $\xi(q^2)$ plus a measured value of ϕ from the time distributions. The predicted ϕ that matches the measured ϕ will correspond to the correct value of $\xi(q^2)$. For the vertical field data, the choices of $\xi(q^2)$

correspond to different values of $Re\xi(q^2)$, with $Im\xi(q^2) = 0.0$. For the horizontal field data, $Im\xi(q^2)$ was varied while $Re\xi(q^2)$ was fixed.

The data are also separated into bands of expected q^2. The q^2 dependence of $\xi(q^2)$ is weak enough that $\xi(q^2)$ can be considered constant over a single band. The data from each band can then be treated in a separate analysis.

B. Event Reconstruction

The raw data tapes from the PDP-9 were analyzed off-line at the Control Data Corporation 7600 computer facility at Lawrence Berkeley Laboratory.

Since the apparatus cannot detect the neutrino or measure the kaon's momentum, the event configuration is kinematically unconstrained. Therefore in the reconstruction program, an event is characterized simply by two tracks, one in each spectrometer arm, that meet at a vertex in the decay region and show continuity through the spectrometer magnets. At this stage, the information from the Cherenkov counters, range device, and polarimeter was not used. Loose cuts were applied for purposes of programming efficiency; the tighter cuts that determine the $K_{\mu 3}$ event sample were applied by a subsequent program, which will be discussed in the next section.

In the initial steps of the reconstruction process, the spark chamber scalers from the SAC units were converted into laboratory coordinates using a continuously updated table of fiducial values (approximately the

average fiducial values from the previous ten events) and the spatial coordinates of the fiducials as determined by a combination of direct measurement and an analysis of tracks from data taken with the magnets turned off. If any chamber (excluding the polarimeter chamber) had no sparks, the event was rejected.

The horizontal hodoscopes were examined, and the event rejected if either of them showed no counter hit. If more than one counter on a side was hit, the program considered each of them in turn.

The spark-sorting process was performed on each arm independently. In the chambers downstream of the magnets, all possible linear trajectories were traced in the x-z plane, with a cut imposed on the computed χ^2 to retain only reasonable possibilites. The y-z plane corridors specified by hits in the horizontal counter hodoscope and the middle spark chamber were then used to help select trajectories in this view. The best straight-line fits in both views were matched and projected to the midplane of the magnets.

All possible rays in the front two chambers were similarly projected to the magnet midplane. A match between front and back within 5 cm horizontally and 2.5 cm vertically specified a trajectory.

Up to three good χ^2 tracks were retained from each side for vertex reconstruction. Projecting a track from each side back into the decay volume, the distance of closest approach was calculated. The closest pair within the liberal fiducial volume was assumed to come from the decay, provided the tracks passed within 5 cm of each other.

C. $K_{\mu 3}$ Event Selections

Assume that, for some event, the reconstruction program determines that there is one unambiguous track in each spectrometer arm. To insure that the event is $K^0_L \rightarrow \pi^- \mu^+ \nu_\mu$ it is sufficient to show that (1) the two tracks originate from the same decay, (2) the track in the pion spectrometer was a pion, and (3) the track in the muon spectrometer was a muon.

Satisfying the first requirement is straightforward. The timing counters ensure that the two tracks occurred within about 10 nanoseconds of each other. The tracks, extrapolated upstream, were required to have a nearest approach of less than 5 cm. The separation at nearest approach has a full width at half maximum of 13 mm, indicating that this cut is quite loose. The point of nearest approach, or vertex, was required to be 7.6 m to 12.7 m from the production target, placing it in the vacuum decay volume. In addition, each track was required to exit the vacuum region via its thin Dacron windows. As the tracks passed through the spectrometer magnets, they were required to miss the magnet walls.

The remaining two requirements require a knowledge of the momenta of the secondaries. This was done with an effective length approximation for the spectrometer magnets,

$$P = \frac{P_t}{\sin\beta_{out} - \sin\beta_{in}}$$

where β_{out} and β_{in} are the secondary's exit and entrant angles in the horizontal plane as measured from the axis of the spectrometer magnet. P_t is the transverse momentum change indicated in Section III-C, obtained from a table as a funcion of position in the magnet aperture. As an indication of the momentum resolution, the full width of the kaon peak in the $m_{\pi\pi}$ distribution was 6 MeV.

To identify the pion, the Cherenkov counter and the range device are used. In the pion spectrometer, a pion signature will be the absence of a Cherenkov signal plus a measured range that is too short for a muon of the measured momentum by at least 2.5 counters (the pion momentum must be greater than 0.56 GeV/c so that the expected muon range is beyond the first counter in the range device). Any inefficiency in these two devices is of concern since it could cause non-$K_{\mu 3}$ events to be accepted. Either an electron missed by the Cherenkov counter or a muon that fell short of its expected range produces a pion signature. The latter condition can occur if the muon scatters out through the sides of the range device. To reduce this probability the track is projected downstream to the z coordinate corresponding to 4 counters past the observed range. This point of the track must be at least 5.1 cm away from the sides of the range device. The rms projected scatter at the rear is approximately 9 cm. The looseness of this cut allows some contamination into the $K_{\mu 3}$ sample, but it is shown in the next section that its effect is minor.

To identify the muons, the Cherenkov counter and the range measured in the polarimeter are used. A muon signature is the absence of a Cherenkov signal plus a range expected of a muon with the measured momentum. If D is the difference between the expected range and the observed range for a muon, then the requirement for a muon signature may be stated as

$$|D| < P_{\mu}/(0.3\ \text{GeV/c})$$

So, for example, a 750 MeV/c muon must stop within 2.5 counters of its expected range. Figure 7 shows the distribution of D for particles entering the polarimeter before and after the other $K_{\mu 3}$ cuts are applied. An additional requirement is that

$$0.66\ \text{GeV/c} < P_{\mu} < 1.04\ \text{GeV/c},$$

corresponding to the momentum acceptance of the polarimeter. The track projected downstream to the expected muon range was also required to be at least 2.54 cm away form the sides of the polarimeter. This compares with the projected rms scatter of about 17 cm at the rear of the polarimeter.

Inefficiencies are not a problem in the muon identification. A true muon that is misinterpreted will cause the event to be thrown out of the analysis. This will affect the statistical precision, but does not bias the answer. A true pion or positron that is incorrectly identified as a muon will not ordinarily produce a delayed signal in the polarimeter and hence will not be included in the analysis.

The additional requirement that a delayed signal be detected in the polarimeter makes the muon identification quite tight. This in turn makes it quite likely that the secondary on the opposite side was indeed a pion. The effects of background channels on the experimental results are considered in Section V-B.

As a check, the transverse cuts in the polarimeter and range device were tightened one at a time. The results for $\xi(q^2)$ were unchanged within the statistical precision.

D. Foundations of the Polarization Measurement

In Part C of Section II it was indicated that the probability density for detecting a decay positron with momentum $\vec{p}$ at time t, from a muon whose polarization is precessing at a frequency ω_L, has the form

$$r(\vec{p},t) = e^{-t/\tau}\left[f'(\vec{p}) + g'(\vec{p})\cos(\omega_L t + \phi_s - \phi_p)\right] ,$$

where ϕ_s and ϕ_p are the initial azimuthal angles of $\vec{s}$ and $\vec{p}$ about $\vec{B}$, and f'and g'are some functions of $\vec{p}$. In the vertical field data, $\vec{B}$ points along the y axis and ϕ is measured in the x-z plane with ϕ= 0.0 corresponding to the positive z axis. The analysis is identical (except for coordinate labels) for the horizontal field data so we will bypass its treatment.

The polarimeter detects positrons in either the downstream ($P_z > 0$) or upstream ($P_z < 0$) hemispheres. This is equivalent to integrating

over infinitessimal detectors covering a halfspace. For example, the probability density for detecting a positron at time t in the forward hemisphere is

$$r^+(t) = \int_{p_z > 0} d^3p\ r(\vec{p},t) = \int_0^{p_{max}} dp \int_0^{\pi} d\theta_p \int_{-\pi/2}^{\pi/2} d\phi_p\ r(\vec{p},t).$$

Assume for a moment that the detection efficiency of the polarimeter is left-right symmetric. Specifically, this means that

$$g'(p,\theta_p,\phi_p) = g'(p,\theta_p,-\phi_p).$$

Then

$$r^+(t) = N^+ e^{-t/\tau}\left[1 + \alpha^+ \cos(\omega_L t + \phi_s)\right],$$

where

$$N^+ \equiv \int_{p_z > 0} d^3p\ f'(\vec{p})$$

and

$$N^+\alpha^+ = \int_{p_z > 0} d^3p\ g'(\vec{p})\cos\phi_p,$$

where α^+ is the asymmetry parameter. But it can be shown [15] that $\alpha^+ = A^+ \cos\theta_s$, where the analyzing power A^+ is independent of $\hat{s}$. Thus

$$r^+(t) = N^+ e^{-t/\tau} \left[1 + A^+ \hat{s}(t) \cdot \hat{z} \right]$$

where

$$\hat{s}(t) \cdot \hat{z} = \cos\theta_s \cos(\omega_L t + \phi_s) \ .$$

An identical argument for the $p_z < 0$ hemisphere gives

$$r^-(t) = N^- e^{-t/\tau} \left[1 - A^- \hat{s}(t) \cdot \hat{z} \right] .$$

Up to now a localized region of the polarimeter around a particular stopped muon has been considered. Now consider a sample of data with a distribution of muons.

Given that the ith muon in the sample has stopped in the polarimeter, let

$$r_i^{\pm}(t) = N_i^{\pm} e^{-t/\tau} \left[1 \pm A_i^{\pm} \hat{s}_i(t) \cdot \hat{z} \right]$$

be the probability density for detecting a positron in the forward or backward hemisphere at time t. Note that

$$\int_0^\infty r_i^{\pm}(t) < 1 ,$$

since not all muon decays are detected.

The positron time distribution accumulated over the entire sample is

$$R^{\pm}(t) \equiv \sum_i r_i^{\pm}(t) = \left(\sum_i N_i^{\pm}\right) e^{-t/\tau} \left\{ 1 \pm \frac{\left[\sum_i N_i^{\pm} A_i^{\pm} \hat{s}_i(t)\right] \cdot \hat{z}}{\sum_i N_i^{\pm}} \right\}.$$

If $R^{\pm}(t)$ is fitted with the parametric form

$$R^{\pm}(t) = N^{\pm} e^{-t/\tau} \left[1 \pm \alpha^{\pm} \cos(\omega t + \phi^{\pm}) \right],$$

the initial phase $\phi^{\pm}$ will equal the azimuthal angle of the vector

$$\vec{V}^{\pm} \equiv \sum_i N_i^{\pm} A_i^{\pm} \hat{s}_i(0),$$

Note that the parameters in the parametric form resemble, but are not the same as previously defined variables. This is meant to be suggestive of the close relationship between corresponding variables and parameters.

The assumption that the polarimeter is uniform and symmetric implies $\vec{V}^{+} = \vec{V}^{-}$ and $\phi^{+} = \phi^{-}$. Indeed, one can think of the two sets of data as two separate experiments measuring the same physical quantity, ϕ. In practice, $R^{+}(t)$ and $R^{-}(t)$ are fitted simultaneously, constraining $\phi = \phi^{+} = \phi^{-}$. In this case, ϕ is expected to equal the azimuthal angle of the vector $\vec{V} = \vec{V}^{+} + \vec{V}^{-}$.

Thus far the possibility of a Poisson-distributed background as well as the consequences of the electronic "logic" of the polarimeter have been neglected. For each pair of adjacent polarimeter counters, the first delayed coincidence, real or spurious, will stop the corresponding scaler. In the off-line analysis, the scalers of the counter pairs immediately upstream and downstream of the muon's stopping point are examined. If delayed signals are indicated in both, but at different times, the scaler with the earliest time is assumed to be real, while the other scaler is ignored.

These complications modify the parameterized time distribution into the form[16]

$$R^{\pm}(t) = e^{-\lambda^{\pm}t}\left\{N^{\pm}e^{-t/\tau}\left[1 \pm \alpha^{\pm}\cos(\omega t + \phi)\right] + \Gamma^{\pm}\right\}. \qquad \text{(IV.1)}$$

Since R^{+} and R^{-} are fitted simultaneously, with $\phi = \phi^{+} = \phi^{-}$, there are 11 parameters: λ^{+}, λ^{-}, N^{+}, N^{-}, τ, α^{+}, α^{-}, ω, ϕ, Γ^{+}, and Γ^{-}. The interpretation of these parameters is that τ is the muon lifetime, $\alpha^{\pm}$ the asymmetry parameter, ω the muon precession frequency, ϕ the initial azimuthal phase of the muon polarization, $N^{\pm}$ the normalization for the real muon signals, $\Gamma^{\pm}$ the background level and $\lambda^{\pm}$ the background frequency. The interpretation of ϕ is unchanged by the random background since the background is uncorrelated with the event configuration.

Other simplified or more complicated parameterizations are possible. However, the phase evaluation is relatively insensitive to different parameterizations (which is not the case with the asymmetry parameter). Tests using other parameterizations showed that the phase was stable to within 10 milliradians. Moreover, these phase variations are generally indifferent to the polarimeter polarity and so would be eliminated by reversing the polarity periodically.

At this point, we have in principal obtained a value ϕ_{measured} for the azimuthal angle of the average initial polarization vector for some data sample. The remaining task is to extract a value for the $K_{\mu 3}$ form factor ξ from ϕ_{measured}. To obtain this relationship, one starts by assuming several a priori values of ξ; then, the Cabibbo-Maksymowicz formula (II.3) and the measured kinematic variables from each event in the actual data-sample are used to compute the expected vector $\vec{V}$ (with expected azimuthal angle ϕ) for each assumed value of ξ, resulting in a table relating ϕ and ξ for this particular data sample. The final value of ξ is obtained by interpolating in this table to the measured value of ϕ. It is important to note that this procedure does not involve Monte Carlo calculations, but instead uses the actual data sample which implicitly contains all the information about acceptance, cuts, biases, etc. for this particular sample.

One difficulty in computing $\vec{V}$ is that $N_i^{\pm}$ and $A_i^{\pm}$ are not known exactly for an individual event. The analyzing power $A_i^{\pm}$ is expected to be quite uniform throughout the polarimeter, since it only depends on the thickness and homogeneity of the aluminum and scintillator plates. The normalization $N_i^{\pm}$, however, depends on the local efficiency of the scintillation counters.

But while the prescription

$$\vec{V} = \sum_i (N_i^+ A_i^+ + N_i^- A_i^-) \hat{s}_i(0)$$

looks impractical, it can be shown[17] that the sum of the polarization vectors from events with a detected positron decay is sufficiently parallel to $\vec{V}$. The restriction to events with detected decays is suggested by the presence of $N_i^{\pm}$ in the weight of $\hat{S}_i(0)$. Two arguments are presented in reference 17. Both arguments use the idea that, while detection-related biases may exist in a single event, such biases will effectively cancel themselves out in a large data sample.

The first argument is based on the property of the polarimeter that "one man's ceiling is another man's floor". A forward decay from a muon in the tenth aluminum plate and a backward decay from a muon in the twelfth plate with the same x-y coordinates involve the same scintillation counters and aluminum plates. N^+ and A^+ for the first muon should equal N^- and A^-, respectively, for the second muon. This is tantamount to saying that $N_i^+ = N_i^-$ and $A_i^+ = A_i^-$ in $\vec{V}$.

The second argument says that if $N_i^{\pm}$ and $A_i^{\pm}$ are uncorrelated with $\hat{S}_i(0)$, then $\vec{V}$ is expected to be parallel to $\sum_i \hat{S}_i(0)$, whether or not the sum is over events with detected positrons. The assumption is valid if the muon's stopping point is independent of its spin. This turns out to be a good assumption, empirically. To first order, the

muon momentum spectrum reflects the kaon momentum spectrum. (The lack of correlation between the spin direction and the transverse stopping position justifies the earlier assumption of left-right symmetry in the detection efficiency. Rather than thinking in terms of a single stopped muon decaying to the left or right, one can imagine a single site in the polarimeter with muons stopping to its left or right).

The final complication in computing $\vec{V}$ is the quadratic ambiguity. The ith muon has two possible polarizations, call them $\hat{S}_{iA}$ and $\hat{S}_{iB}$. However, it is possible to determine the probabilities for each vector[18], call them P_{iA} and P_{iB}. The expected polarization of the ith muon is then

$$\langle \vec{s}_i \rangle = P_{iA}\hat{S}_{iA} + P_{iB}\hat{S}_{iB}.$$

Also, since

$$\langle \sum_i \hat{S}_i \rangle = \sum_i \langle \hat{S}_i \rangle,$$

the sum of $\langle \hat{S}_i \rangle$ over a sample of events is the expected value of $\Sigma \hat{S}_i$. A statistical error for ϕ results from using $\sum_i \langle \hat{S}_i \rangle$ as an estimator of ΣS_i, with a binomial-like distribution in each component.[19]

E. Procedure

The flow diagram in figure 8 summarizes the analysis scheme. The raw data are filtered by cuts to yield a data sample of presumed $K_{\mu 3}$ events. The $K_{\mu 3}$ sample is further restricted to include only events that indicate a muon decay in the polarimeter. These can then be distributed into bins of q^2.

From this point in the analysis, each event is handled along two separate lines.

Using the polarimeter information, the event is binned in the appropriate time distribution. When the data processing is completed, the time distributions are fitted with an 11 parameter function to yield ϕ_{exp}, the experimentally measured value of the azimuthal phase angle of $\sum_i \hat{S}_i$.

Using the spectrometer information, the expected polarization vector is computed with six different values of Reξ or Imξ: -0.5, -0.3, -0.1, 0.1, 0.3, 0.5. To compute the polarization of the muon in the polarimeter, the Cabibbo-Maksymowicz formula is used which gives the polarization as seen in the muon's rest frame, but expressed in laboratory coordinates. Because the Lande factor is g = 2 for the muon (the small deviation is negligible), the Cabibbo-Maksymowicz result must be rotated by the same angle as the muon momentum vector in passing through the spectrometer magnet. Ray tracing programs show that depolarization caused by magnetic field components parallel to the momentum vector is negligible. Muons also do not depolarize in the process of slowing down.[20]

The six vectors are accumulated with the corresponding vectors from other events in the sample. When the data processing is completed, the six accumulated vectors yield six values of $\phi_{pred}(\xi_i)$ $(i = 1,\ldots,6)$, the predicted azimuthal phase angle of $\sum_i (P_{iA}\hat{S}_{iA} + P_{iB}\hat{S}_{iB})$ for six a priori choices of $\xi(q^2)$.

If the true value of $\xi(q^2)$ had been used in computing $\phi_{pred}(\xi)$, then $\phi_{pred}(\xi_{true}) = \phi_{exp}$. In practice the process is reversed. From

the curve $\phi_{pred}(\xi)$ the inverted function $\xi(\phi_{pred})$ is obtained. Then $\xi_{true} = \xi(\phi_{exp})$.

The determination of ϕ_{exp} presumes that the time origin is known. However, there is some delay from the time the muon comes to rest before the scaler gates are opened. One way around this is to reverse the polarimeter field periodically and analyze the data from the two polarities separately in the manner outlined above. This results in two experimental phases $\phi_{exp}^{\uparrow}$ and $\phi_{exp}^{\downarrow}$. The results are combined to get

$$\phi_{exp} = \frac{1}{2}(\phi_{exp}^{\downarrow} - \phi_{exp}^{\uparrow})$$

Any phase shift caused by an incorrect zero-time now cancels out, leaving ϕ_{exp} unaffected. In fact, the zero-time phase shift can be derived by

$$\Delta\phi = \frac{1}{2}(\phi_{exp}^{\uparrow} + \phi_{exp}^{\downarrow})$$

The zero-time phase shift was also measured directly by the polarimeter electronics, with excellent agreement to the fitted phase results.

F. Statistics

The most important contribution to the statistical error of ξ is, of course, the error in measuring ϕ from the time distributions. In fitting for ϕ with the parametric form given by (IV.1), it turns out that ϕ is highly correlated with ω, but essentially uncorrelated

with all other parameters. (This is also true in the expanded parametric form which provides for a Poisson background and the simultaneous fitting of the upstream and downstream distributions.)

If there are $M \equiv \int_{t_1}^{t_2} R(t)dt$ detected positrons in the data sample (where the scaler gate is open from t_1 to t_2) and if ω is known precisely then the expected error in ϕ is

$$\sigma_\phi = \frac{\sqrt{2}}{\alpha\sqrt{M}}$$

But, if ω is another parameter, the expected error in ϕ becomes

$$\sigma_\phi = \frac{\sqrt{2}}{\alpha\sqrt{M}} \cdot \frac{1}{\sqrt{1-\rho^2}}$$

where ρ is the correlation coefficient between ϕ and ω. With $\rho \cong 1/\sqrt{2}$ the error in ϕ increases by 41%.

It is unnecessary to independently measure ω since the error in fitting the combined data (all q^2 bands lumped together) for ω is comparable to the reproducibility of a conventional flip coil of about 0.2%. Moreover, there are variations with position of the polarimeter field strength of as much as $\pm 0.5\%$, which would necessitate a cumbersome field map as well as open the door to systematic uncertainties.

When the data are divided according to q^2, however, some of the bands may contain only a small fraction of the events. In this case, it will pay to fix the frequency at the value obtained from the lumped data

sample, with its correspondingly smaller error. For each band of q^2, the expected error in ϕ will then be given by

$$\sigma_\phi^2 = \sigma_1^2 + \rho^2\sigma_2^2$$

where σ_1 is the error in ϕ if ω were known exactly and σ_2 is the error in ϕ in the lumped data sample.

An additional minor contribution to the statistical error comes from the uncertainty in the predicted phase caused by the quadratic ambiguity (see Part D of this section). This error is added in quadrature to the preceeding contributions.

For the phase analysis of this experiment, the data were in the form of two time distributions. The time dimension was quantized into 20 nanosecond bins by the 50 Megahertz clock. For convenience the data were further consolidated into 80 nanosecond time bins. A Monte Carlo study of the statistical precision of the phase as a function of the time binning showed (see Figure 9) that there is virtually no loss of precision from this consolidation. (Note that 80 nanoseconds is $0.036\tau_\mu$ and corresponds to an angular rotation by the polarization of 39 degrees). Together, the two distributions contained 148 time bins which were used to fit the 11 parameter function of equation IV.1.

V. RESULTS

A. Results of the Analysis Procedure

$Re\xi(q^2)$ is determined using the data with the precessing field pointing in the vertical direction. A total of 19 million triggers were recorded in this configuration. In about 75 percent of the triggers, there was a reconstructed track in both spectrometer arms. After imposing the vertex requirements, about 63 percent of the triggers remained as reconstructed events. In about 35 percent of these events, the two secondary tracks were identified as a μ^+ and a π^-. After applying further $K_{\mu 3}$ cuts (mainly that the secondaries terminate in the range device or polarimeter), and requiring an apparent muon decay in the polarimeter, about 350,000 events remain, representing 1.8 percent of the triggers. Further cuts, mainly the limits on the secondaries' momenta, reduce the sample to the final total of 207, 260; 110,648 events with the polarimeter magnetic field pointing in the -y direction, and 96,612 events with the field in the +y direction.

Figures 10a through 10d show the time distributions for the upstream and downstream decays for two polarities of the polarimeter field. The results of the parameterized fits are presented in Table I. The asymmetry is about 0.32, in agreement with our design calculation.

The result of separating the data into bands of q^2 and fixing the precession frequency is presented in Table II. The curves of ϕ_{pred} versus ξ for the various q^2 bands are shown in figure 11.

This gives, finally, the results for $\xi(q^2)$ (where q^2 is the average for the events in each band), which are presented in Table III and figure 12. Figure 13 shows the data re-expressed in terms of f_0/f_+. The results of Donaldson, et al.[1], are indicated by the solid line in the same figure.

If one parameterizes the q^2 dependence of ξ by

$$\xi(q^2) = \xi(0) + \Lambda q^2/m_\pi^2 \quad ,$$

then

$$\xi(0) = 0.51 \pm 0.55 ,$$

$$\Lambda = -0.09 \pm 0.14 ,$$

with a correlation of -0.981. The regression line for $\xi(0)$ is given by

$$\xi(0) = 0.178 \pm 0.105 - 3.80\ \Lambda \ .$$

To compare this result with those from other polarization experiments, one takes Λ=0 (see page 49 of Reference 2), giving $\xi(0)=0.178 \pm 0.105$.

To determine $Im\xi(q^2)$, the data with the precessing field pointing in the horizontal direction (along the x axis) are used. In this configuration, a total of 5.7 million triggers were collected. Since the spectrometer and $K_{\mu 3}$ cuts are unchanged drom the vertical field configuration, the event attrition rates are the same. The final sample contained 25,682 events with the polarimeter field in the -x direction and 29,922 events with the field in the +x direction.

Figures 14a through 14d show the time distributions for these data.

The results of the parameterized fits for the horizontal field data are presented in Tables IV and V. The curves of ϕ_{pred} as a function of $Im\xi(q^2)$ are shown in Figure 15. The resulting values for $Im\xi(q^2)$, with $Re\xi(q^2)$ fixed at 0.0 are presented in Table VI. The sensitivity of the determination of $Im\xi(q^2)$ to the assumed value of $Re\xi(q^2)$ was measured by reanalyzing the data with $Re\xi(q^2) = -0.5$. The results of this reanalysis are presented in Table VII. If $Im\xi(q^2)$ has little or no q^2 dependence then $Im\xi = 0.352 \pm 0.297 + 0.206\ Re\xi$ ($\chi^2 = 4.02$ for 4 degrees of freedom).

B. Systematics

The results presented in Section A depend on correct values for several parameters that are assumed in the analysis. To see their effects on $Re\xi$ each of these parameters has been varied in turn, and the analysis repeated.

The results of this procedure are summarized in Table VIII. The statistical errors from Section A are shown for comparison. All effects are less than 10% or so of the statistical error. All of the parameter shifts indicated are larger than they are expected to be. The magnets were calibrated to better than 0.1% by using the $K^0_L \to \pi^+\pi^-$ events in the data with the constraints imposed by the target position and the $\pi\pi$ invariant mass. The K^0_L momentum spectrum, used in computing the relative weights of the two ambiguous solutions, was obtained by examining a sample of 120,000 $K^0_L \to \pi^+\pi^-$ events from a previous run with the same spectrometer. A skewing error in the momentum spectrum (one that enhances one side of the spectrum at the expense of the other) will bias one solution over the other. Two independently written Monte Carlo

programs produced the identical spectrum. A skewing error of as much as 1.0% per GeV/c can be ruled out.

Radiative corrections are also negligible. Ginsberg and Smith[21] have calculated that the percentage change in the transverse component of the polarization is less than 0.25% in the region of the Dalitz plot examined in this experiment. Also, the quadratic ambiguity reduces any sensitivity to the radiative corrections by roughly a factor of 1/3 for the same reason that it reduces the sensitivity to ξ. This reduces the maximum expected angular shift to less than 1 milliradian, which is negligible.

Finally, the possibility of contamination of the $K_{\mu 3}$ sample by other event types is considered. Only contaminations with real muons entering the polarimeter will influence the results and then only if the muons are polarized. This is possible if a π^+ decays in flight on the polarimeter side. Calculations indicate that approximately 2% of the positive pions from the various detected kaon decay modes will decay in flight and will be misidentified as a muon. We discuss below the various backgrounds involving pion decay in flight with the daughter muon stopping in the polarimeter.

1. $\underline{K^0_L \to \pi^+\pi^-}$

The number of $K^0_L \to \pi^+\pi^-$ decays seen is about 1% of the number of $K_{\mu 3}$ events. The fraction of $K^0_L \to \pi^+\pi^-$ decays that decay in flight and pass the muon range cut is calculated to be less than 10%. Hence any effect will be below the 1 milliradian level.

2. $K^0_L \to \pi^+\pi^-\pi^0$

The $K^0_L \to \pi^+\pi^-\pi^0$ mode is suppressed by the relatively high transverse momentum requirement of the muon spectrometer. The maximum transverse momentum in a $K^0_L \to \pi^+\pi^-\pi^0$ decay is 0.133 GeV/c. With a subsequent π^+ decay, this reaches 0.163 GeV/c. Figure 16 shows the $(p'_0)^2$ distribution from this experiment. The variable p'_0 is the K^0_L momentum in the center-of-momentum frame of the two charged secondaries, under the assumption that the event is $K^0_L \to \pi^+\pi^-\pi^0$. The presence of $K^0_L \to \pi^+\pi^-\pi^0$ events in the data would appear as a narrow structure with $(p'_0)^2 \geq 0.0$, apart from resolution effects, tailing off exponentially on the positive side. No such structure is detectable.

3. $K_{\mu 3}$ with Reversed Charges

In this case, the muon must be mistaken for a pion by the range device, most likely as a result of scattering out through the sides. If the range device were totally efficient, these events would appear to have muons in both spectrometer arms. Combining all events which are interpreted as having muons in both arms with the selected $K_{\mu 3}$ sample augments the reversed charge contamination. This corresponds to the range device always misidentifying a muon as a pion. The analysis is repeated to observe any shift in ξ (see Table IX). This gives a second point on the curve of ξ as a function of range device efficiency. While the actual efficiency is not known exactly, it is conservatively estimated to be better than 90%. The value of ξ for a totally efficient range device (which excludes $K_{\mu 3}$ events with reversed charges) is then expected to differ from the observed ξ by <10% of the shifts in Table IX.

4. K_{e3}

In this case, the electron is missed by the Cherenkov counter. Following the lead of the previous paragraph, consider events interpreted as having a muon in the polarimeter with an electron on the other side. These events are combined with the $K_{\mu 3}$ sample to observe any shift in ξ. The Cherenkov counter is shown to be at least 95% efficient by examining events with a well defined pion in the polarimeter and no muon in the range device. Five percent of this shift is taken as an upper limit.

The results of the procedure outlined in Subsections 3 and 4 above are shown in Table IX. The implied corrections to ξ are small compared to the statistical error.

C. Concluding Remarks

In this experiment no Monte Carlo simulation is required except to get the K^o_L momentum spectrum from the two body $K^o_L \to \pi\pi$ decays. The results do not depend on the $K_{\mu 3}$ cuts since the important consideration is that the time distributions and the predicted phases are derived from the same data sample. The results are not sensitive to dead spots or counter inefficiencies in the polarimeter since the stopping point of a muon is largely uncorrelated with its spin. (If a positron emitted upstream were mistaken for a downstream emission because of counter inefficiencies, the asymmetry would be degraded but no bias in the phase would result). The polarimeter does not need to have a very uniform magnetic field. The analysis allows the frequency to vary as a parameter, and the resulting value represents the average frequency over that particular data sample. When events with a higher-than-average frequency are combined with those having a lower-than-average

frequency, the resultant vector precesses at the mean frequency with its initial phase undisturbed. Since the field was uniform to 0.5%, the apparent depolarization was less than 1% in the worst case.

ACKNOWLEDGMENTS

We thank Drs. William A. Wenzel and Henry J. Frisch for their interest and participation during the initial stages of the experiment. Gerry Schnurmacher and Arthur Zingher also lent general assistance.

Much of the physical effort involved in setting up and running this experiment was handled by our technicians. In particular, we would like to thank William Baldock for his assistance in mapping the polarimeter magnetic field; Katherine Lucas in the mapping of the spectrometer magnets, and John Wilson in programming the PDP-9. Others were Fred Goozen, Timothy Nuzum, and Tom Weber. We would also like to thank Dr. Hermann Grunder and the Bevatron operators for providing us with a reliable and RF-free proton beam.

REFERENCES

* Work done under the auspices of the U.S. Energy Research and Development Administration

**Present Address: Stanford Linear Accelerator Center, Stanford, CA 94305

† Present Address: Fermi National Accelerator Laboratory, Batavia, IL 60510

1. G. Donaldson, D. Fryberger, D. Hitlin, J. Liu, B. Meyer, R. Piccioni, A. Rothenberg, D. Uggla, S. Wojcicki, and D. Dorfan, Phys. Rev. Lett. 31, 337 (1973).
2. Particle Data Group, Review of Particle Properties, Phys. Lett, 50B, 1 (1974).
3. M.K. Gaillard and L.M. Chounet, CERN 70-14, 29 (1970).
4. T.D. Lee and C.S. Wu, Ann. Rev. of Nucl. Sci. 16, 476ff (1966).
5. N. Cabibbo and A. Maksymowicz, Phys. Lett. 9, 352 (1964); 11, 360 (1964); 14, 72 (1965).
6. A.O. Weissenberg, Muons (North Holland Pub. Co., Amsterdam, 1967), p. 47.
7. H.J. Frisch, Stringent Limits on the Decays $K^0_L \to \mu^+\mu^-$, e^+e^-, $\mu^\pm e^\mp$, (Ph.D. Thesis), UCRL-20264, March 1971 (unpublished).
8. D.E. Coyle, R.C. Field, J.T. Gunn, and J.T. Tanabe, Nucl. Inst. and Meth. 95, 557 (1971).
9. R.C. Field, Bev-1039 (Internal document of the LBL Accelerator Division unpublished).
10. R. Johnson and G. Shen, Addendum to Bev-3030 (Internal document of the LBL Accelerator Division, unpublished).

11. R.C. Weast, Handbook of Chemistry and Physics, (The Chemical Rubber Co., Cleveland, Ohio, 1965), 46th Edition, p. E-95.

12. Proceedings of the Meeting on Muons in Solid State Physics, Burgenstock, 87 (1971).

13. D.G. Andrianov, G.G. Myasishcheva, Yu. V. Obukhov, V.S. Roganov, V.G. Firsov, and V.I. Fistul, Soviet Physics JETP 29, 643 (1969).

14. Lawrence Radiation Laboratory Counting Handbook, UCRL-3307 revised edition (unpublished).

15. G. Shen, Determination of the $K^0_L \to \pi^- \mu^+ \nu_\mu$ Form Factor $\xi(q^2)$ by Muon Polarization Measurements, (Ph.D. Thesis), LBL-4275, Appendix A, September, 1975 (unpublished); Also see A.R. Clark, R.C. Field, W.R. Holley, R.P. Johnson, L.T. Kerth, R.C. Sah, and G. Shen, Determination of the $K^0_L \to \pi^- \mu^+ \nu_\mu$ Form Factor $\xi(q^2)$ by Muon Polarization Measurements, LBL-4802, Appendix A, January 1976 (unpublished).

16. Ibid, Appendix B.

17. Ibid, Appendix C.

18. Ibid, Appendix D.

19. Ibid, Appendix E.

20. A. Buhler, T. Massam, Th. Muller, M. Schneegans, and A. Zichichi, Il Nuovo Cimento 39, 824 (1965).

21. E.S. Ginsberg and J. Smith, Phys. Rev. D8, 3887 (1973).

TABLE I. PARAMETERIZED FIT TO VERTICAL FIELD DATA WITH ALL q^2 BANDS COMBINED

Parameter	units	Pol. Field Up	Pol. Field Down
N^-		1909 ± 57	2079 ± 92
N^+		1454 ± 37	1619 ± 42
α^-		0.264 ± 0.015	0.293 ± 0.022
α^+		0.315 ± 0.016	0.322 ± 0.018
ϕ	radians	-0.719 ± 0.033	0.705 ± 0.029
ω	10^6 rad/sec	8.304 ± 0.015	8.387 ± 0.014
τ	10^{-6} sec.	2.26 ± 0.14	2.31 ± 0.12
Λ^-		193 ± 60	323 ± 93
Λ^+		132 ± 39	175 ± 47
λ^-	10^3	71 ± 40	107 ± 38
λ^+	10^3	42 ± 38	54 ± 33
χ^2/DOF		124.9/137	190.0/137[a]
$\rho_{\phi\omega}$		-0.787	-0.776

[a]The purpose of this first fit (with all q^2 bands lumped together) is only to determine ω. The poor χ^2 here is caused by a few pathological bins at very early times, which apparently do not affect the frequency determination. By starting the fit from a later time bin, a frequency of $(8.382 \pm 0.023) \times 10^6$ rad/sec was obtained with a χ^2 of 107.5 for 109 degrees of freedom.

TABLE II. PHASE ANGLES FROM VERTICAL FIELD FIT TO INDIVIDUAL q^2 BANDS (ω FIXED)

Polarimeter Field	q^2/m^2_π	χ^2 (138 DOF)	Polarization Phase [a]
Down	4.45	129.0	$0.9283^{+0.0868}_{-0.0866}$
Down	3.45	186.0	$0.7807^{+0.0456}_{-0.0453}$
Down	2.45	148.1	$0.6923^{+0.0349}_{-0.0348}$
Down	1.44	150.9	$0.6688^{+0.0282}_{-0.0281}$
Down	0.84 [b]	127.5	$0.5244^{+0.0674}_{-0.0672}$
Up	4.45	141.3	$-0.9944^{+0.0910}_{-0.0918}$
Up	3.45	143.8	$-0.8583^{+0.0508}_{-0.0510}$
Up	2.45	145.6	$-0.7389^{+0.0377}_{-0.0378}$
Up	1.44	143.9	$-0.6921^{+0.0300}_{-0.0301}$
Up	0.84 [b]	155.5	$-0.6029^{+0.0638}_{-0.0638}$

[a] Phases not corrected for possible zero-time error. See Section IV, Part E.

[b] Not used in final analysis (Table 4) because of large phase error and virtually no sensitivity to ξ.

TABLE III DETERMINATION OF $\xi(q^2)$

q^2/m_π^2	Polarization Phase	$\xi(q^2)$
1.439	$0.6489\ ^{+0.0269}_{-0.0268}$	$0.455\ ^{+0.941}_{-0.913}$
2.452	$0.7156\ ^{+0.0310}_{-0.0309}$	$0.204\ ^{+0.294}_{-0.301}$
3.448	$0.8195\ ^{+0.0385}_{-0.0382}$	$0.265\ ^{+0.171}_{-0.180}$
4.445	$0.9614\ ^{+0.0660}_{-0.0654}$	$0.104\ ^{+0.141}_{-0.154}$

TABLE IV PARAMETERIZED FIT TO

HORIZONTAL FIELD DATA WITH ALL q^2 BANDS COMBINED

Parameter	+x Field	-x Field
ϕ-ω Correlation	-0.776	-0.759
Phase Error (mrads)	±71.73	±73.73
Frequency ω (10^6 rad/sec)	8.267±.035	8.265±.040
χ^2/DOF	152.0/137	119.1/137

TABLE V PHASE ANGLES FROM HORIZONTAL FIELD

FIT TO INDIVIDUAL q^2 BANDS (ω FIXED)

Polarimeter Field	q^2/m^2_π	χ^2 (138 DOF)	Polarization Phase[a] (milliradians)
-x	4.44	142.2	3.4±370.3
-x	3.45	115.5	44.1±111.1
-x	2.45	106.7	-223.3± 93.3
-x	1.44	125.4	-138.8± 75.2
-x	0.84	127.8	-130.6±141.7
+x	4.44	135.8	-290.9±295.6
+x	3.45	128.6	47.4±116.2
+x	2.45	126.5	36.8± 85.7
+x	1.44	127.1	2.3± 64.4
+x	0.84	116.2	-85.3±141.3

[a] Phases not corrected for possible zero-time error.

TABLE VI DETERMINATION OF $Im\xi(q^2)$

q^2/m^2_π	Polarization Phase (milliradians)	$Im\xi(q^2)$
4.44	-147.15 ± 240.17	-0.209 ± 0.559
3.45	1.65 ± 89.55	0.197 ± 0.428
2.45	130.05 ± 74.63	1.236 ± 0.646
1.44	70.55 ± 63.31	2.183 ± 1.868
0.84	22.65 ± 107.56	-2.342 ±13.821

TABLE VII SENSITIVITY OF $Im\xi(q^2)$ TO $Re\xi(q^2)$

q^2/m^2_π	Shift in $Im\xi(q^2)$ [a]
4.44	-0.142
3.45	-0.106
2.45	-0.040
1.44	-0.119
0.84	0.432

[a] $Im\xi$ for $Re\xi = -0.5$ minus $Im\xi$ for $Re\xi = 0.0$.

TABLE VIII SENSITIVITY OF Re (q^2) TO POTENTIAL SYSTEMATIC ERRORS

	Bin of q^2				
q^2/m^2_π	1.44	2.45	3.45	4.45	All
Statistical Error of $\xi(q^2)$	0.92	0.30	0.18	0.14	0.105
p_π raised 1%	-0.012	+0.007	-0.002	-0.014	-0.005
p_π lowered 1%	-0.035	-0.003	-0.002	+0.006	+0.001
p_μ raised 1%	+0.084	+0.016	+0.019	-0.015	+0.006
p_μ lowered 1%	-0.135	-0.029	-0.004	+0.003	-0.008
λ_+ set at 0.01	-0.018	+0.001	+0.020	+0.007	+0.011
λ_+ set at 0.02	-0.010	+0.001	+0.010	+0.003	+0.005
+5%/Gev ramp in p_K	+0.067	+0.043	+0.040	+0.031	+0.038
-5%/Gev ramp in p_K	-0.082	-0.044	-0.047	-0.035	-0.042

TABLE IX UPPER LIMIT CORRECTIONS TO $Re\xi(q^2)$

FROM CONTAMINATION OF THE $K_{\mu 3}$ SAMPLE

q^2/m^2_π	$Re\xi(q^2)$	$\Delta\xi$ for 90% efficient range device	$\Delta\xi$ for 95% efficient Cherenkov counter
1.44	0.45 ± 0.92	-0.031	-0.021
2.45	0.20 ± 0.30	-0.008	-0.012
3.45	0.26 ± 0.18	-0.002	-0.009
4.45	0.10 ± 0.14	-0.011	-0.010
All	0.178 ± 0.105	-0.007	-0.010

FIGURE CAPTIONS

Fig. 1 Diagram of $K^0_L \to \pi^- \mu^+ \nu_\mu$

Fig. 2 (a) Contours indicating the relative phase space population of the $K_{\mu 3}$ Dalitz plots for $Im\xi = 0$ and $Re\xi = 0$.

(b) Contours indicating the relative acceptance of the apparatus over the Dalitz plot. The x indicates the optimum point for polarization measurements, as defined in the text.

Fig. 3 Plan view of the apparatus. T are the timing counters, H are the horizontal hodoscopes, F & R are the front and rear vertical hodoscopes.

Fig. 4 The range device and Cherenkov counter in the pion spectrometer.

Fig. 5 Schematic view of a section of the polarimeter interior, showing several scintillation counters and aluminum plates.

Fig. 6 Delayed signal interpretation in the polarimeter. The vertical lines represent scintillation counters. If one imagines time flowing downwards, then the x's indicate which counters produced a signal at various times. The muon enters from the left.

Fig. 7 Difference (D) between expected and actual ranges for particles stopping in the polarimeter, divided by the measured momentum. The arrows indicate the location of the cut for this distribution. The upper distribution occurs before, and the lower after, the other $K_{\mu 3}$ cuts.

Fig. 8 Flow diagram of the analysis procedure.

Fig. 9 Monte Carlo result indicating the statistical phase error expected from the parameterized fit as a function of the time resolution.

Fig. 10 Frequency versus time for decays in the polarimeter with the vert-

ical magnetic field. The top half is a linear scale for comparing the goodness of fit at early times, while the lower half is a logarithmic scale for comparison at later times. (a) Polarimeter field pointing down, positron emitted in the upstream hemisphere. (b) Field down; downstream decay. (c) Field up; upstream decay. (d) Field up; downstream decay.

Fig. 11 Predicted polarization phase as a function of ξ for various bands of q^2.

Fig. 12 The form factor $\xi(q^2)$.

Fig. 13 The result of this experiment expressed as $f_0(q^2)/f_+(0)$. For comparison, the solid line shows the result of Donaldon, et al. (Reference 1).

Fig. 14 Frequency versus time for decays in the polarimeter with the horizontal magnetic field. The top half is a linear plot, while the lower half is a logarithmic plot: (a) Polarimeter field pointing in the -x direction, positron emitted in the upstream hemisphere; (b) -x field, downstream decay. (c) +x field, upstream decay; (d) +x field, downstream decay.

Fig. 15 Predicted polarization phase as a function of Imξ for various bands of q^2.

Fig. 16 Event frequency versus $(p_0')^2$.

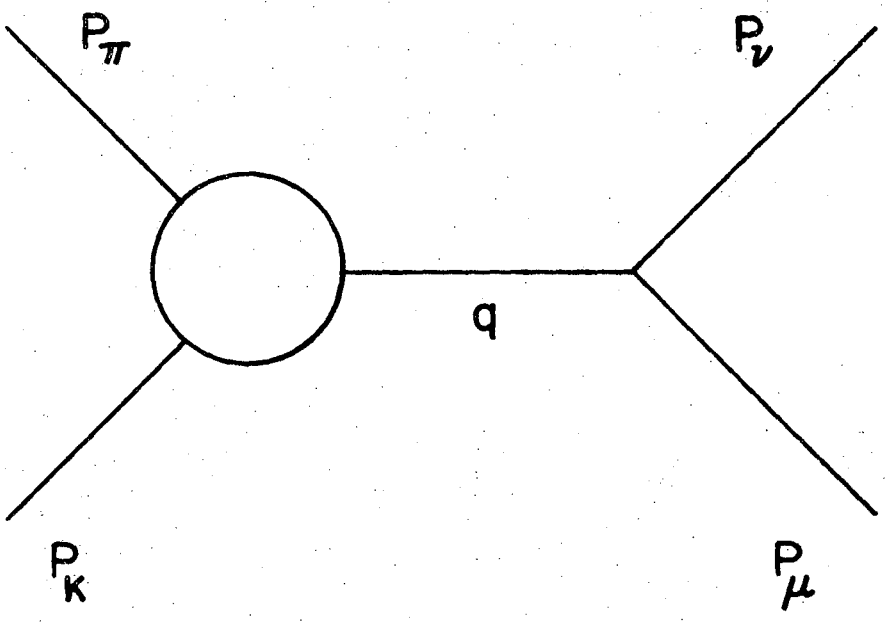

XBL 759-8191

Fig. 1

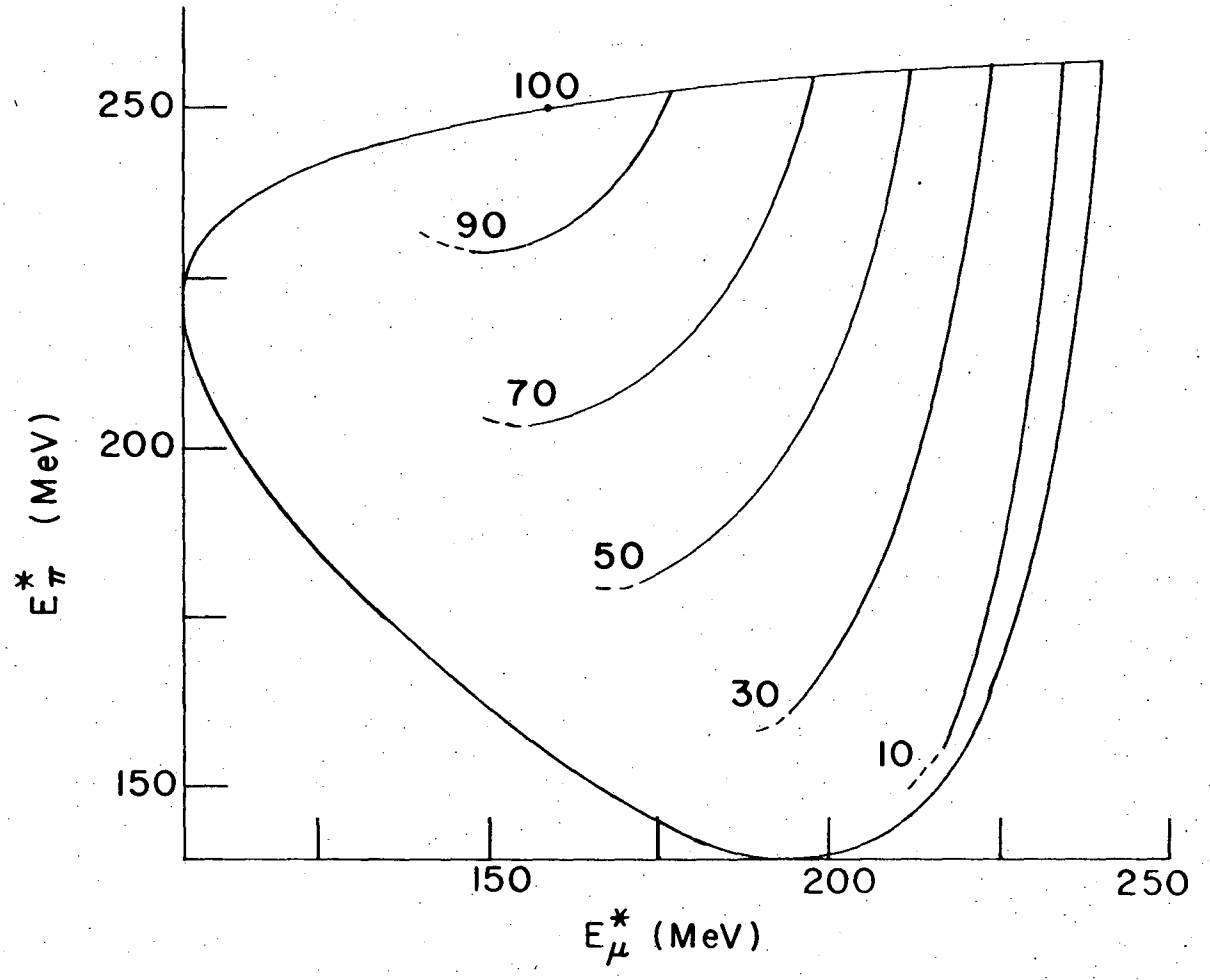

XBL 759-8188

Fig. 2a

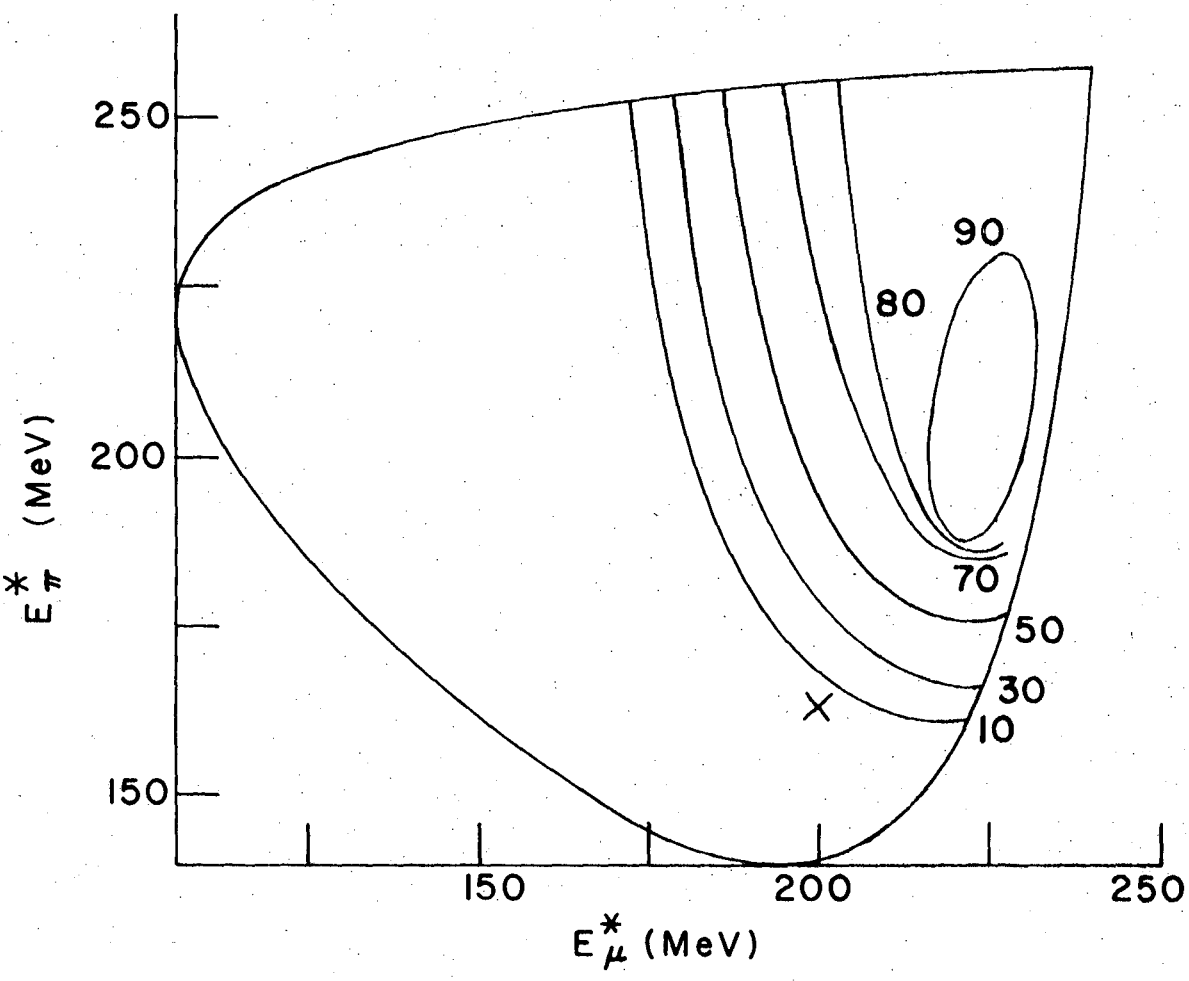

XBL 759-8187

Fig. 2b

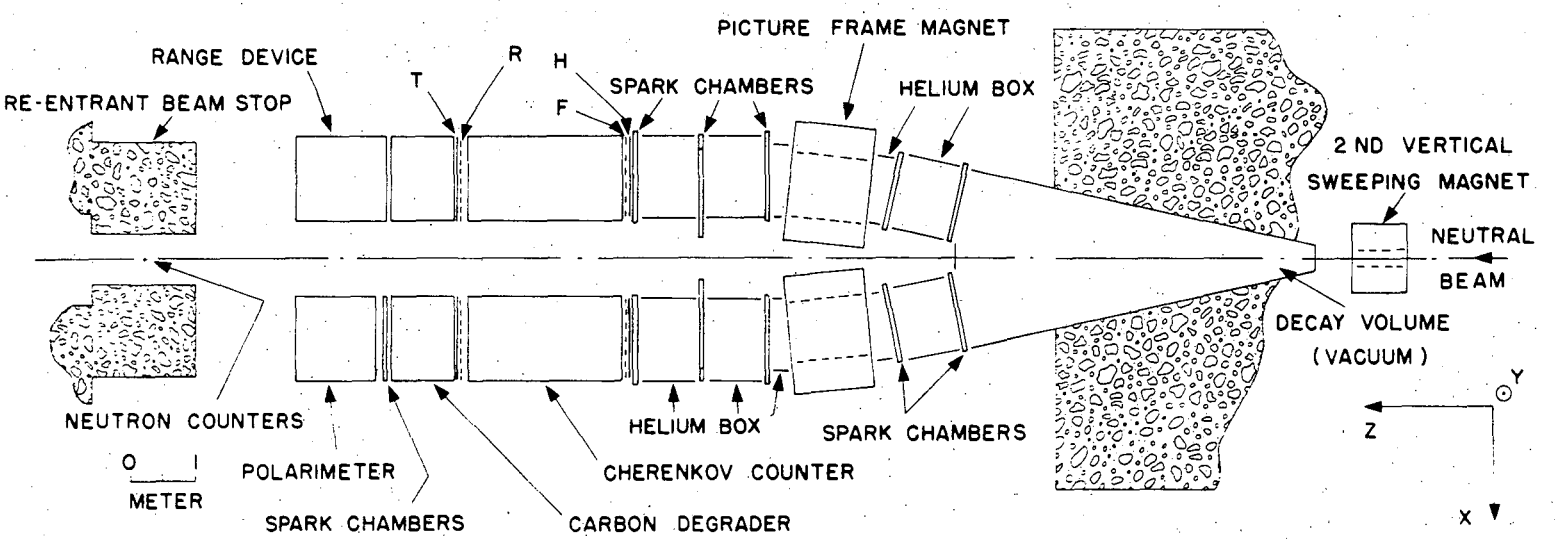

XBL 702-315B

Fig. 3

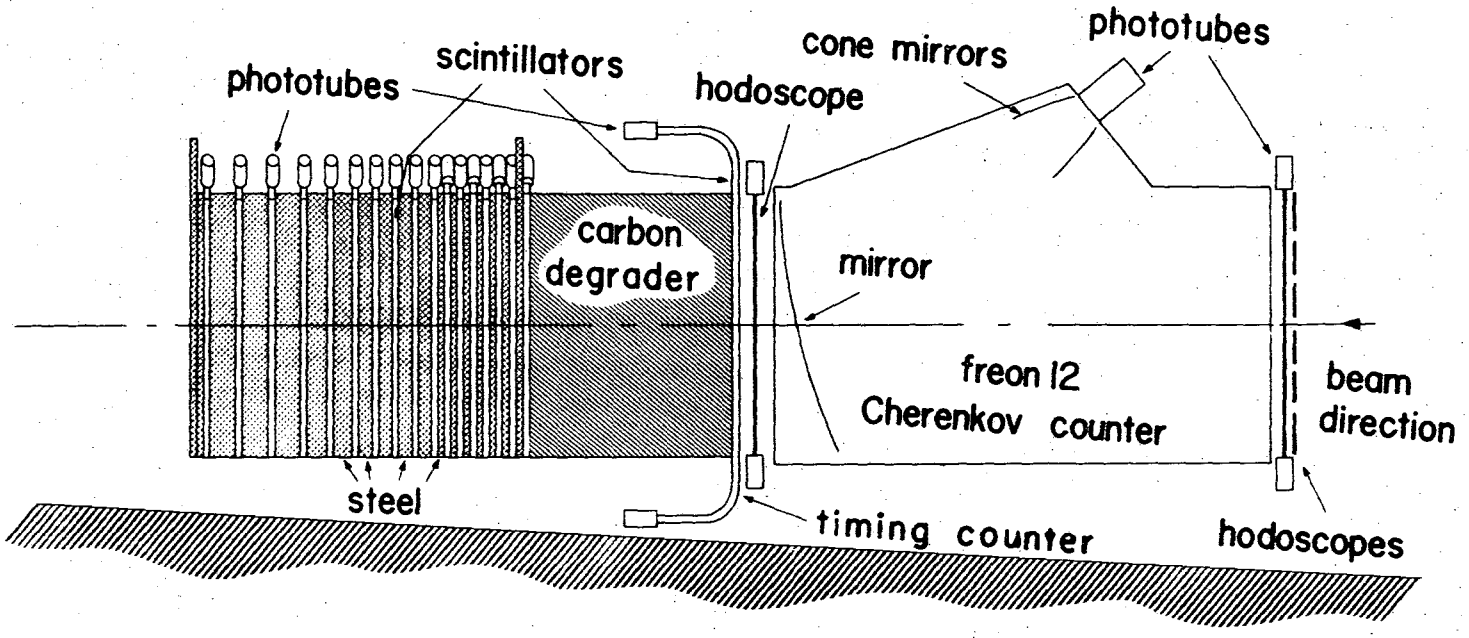

XBL 702-316A

Fig. 4

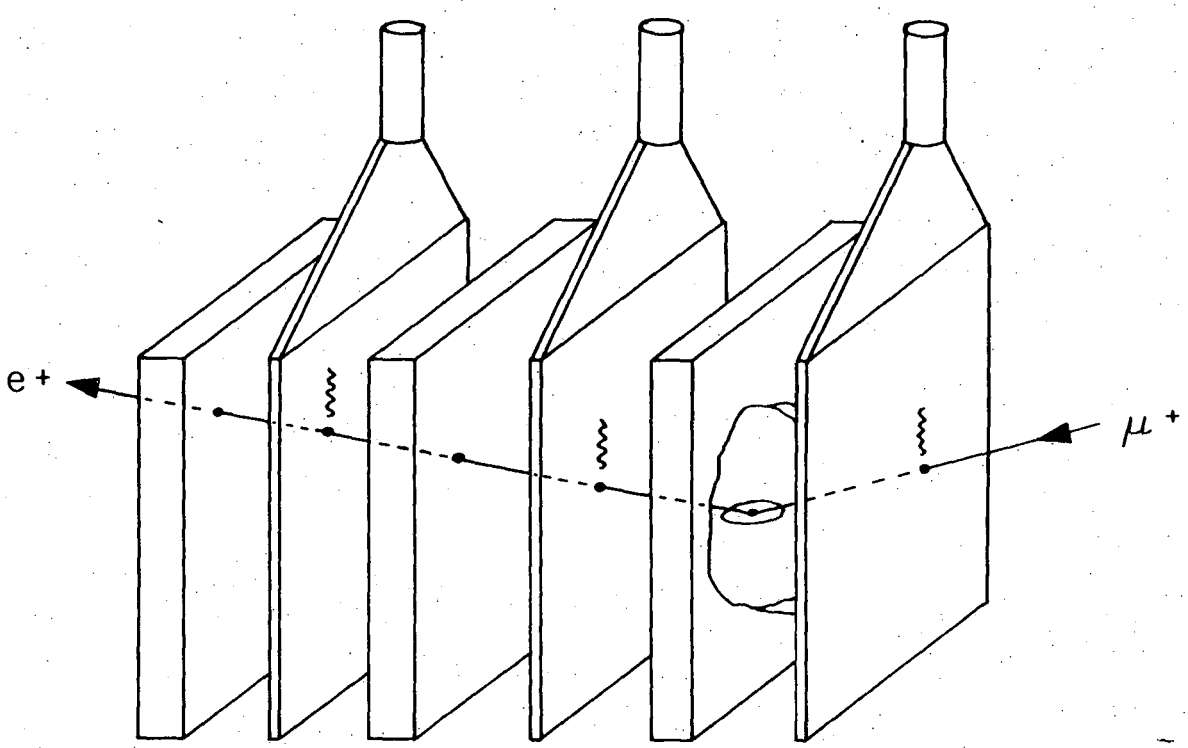

XBL 759-8189

Fig. 5

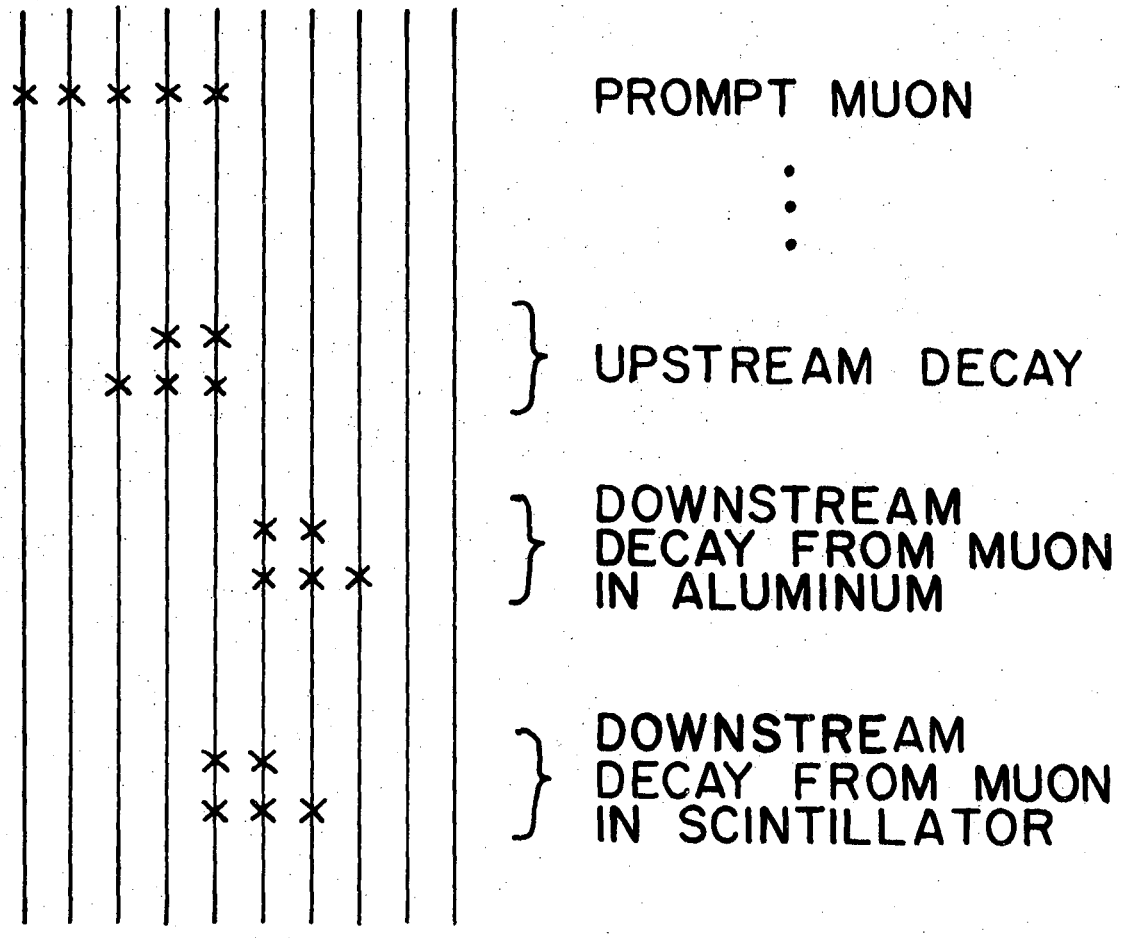

XBL 759-8194

Fig. 6

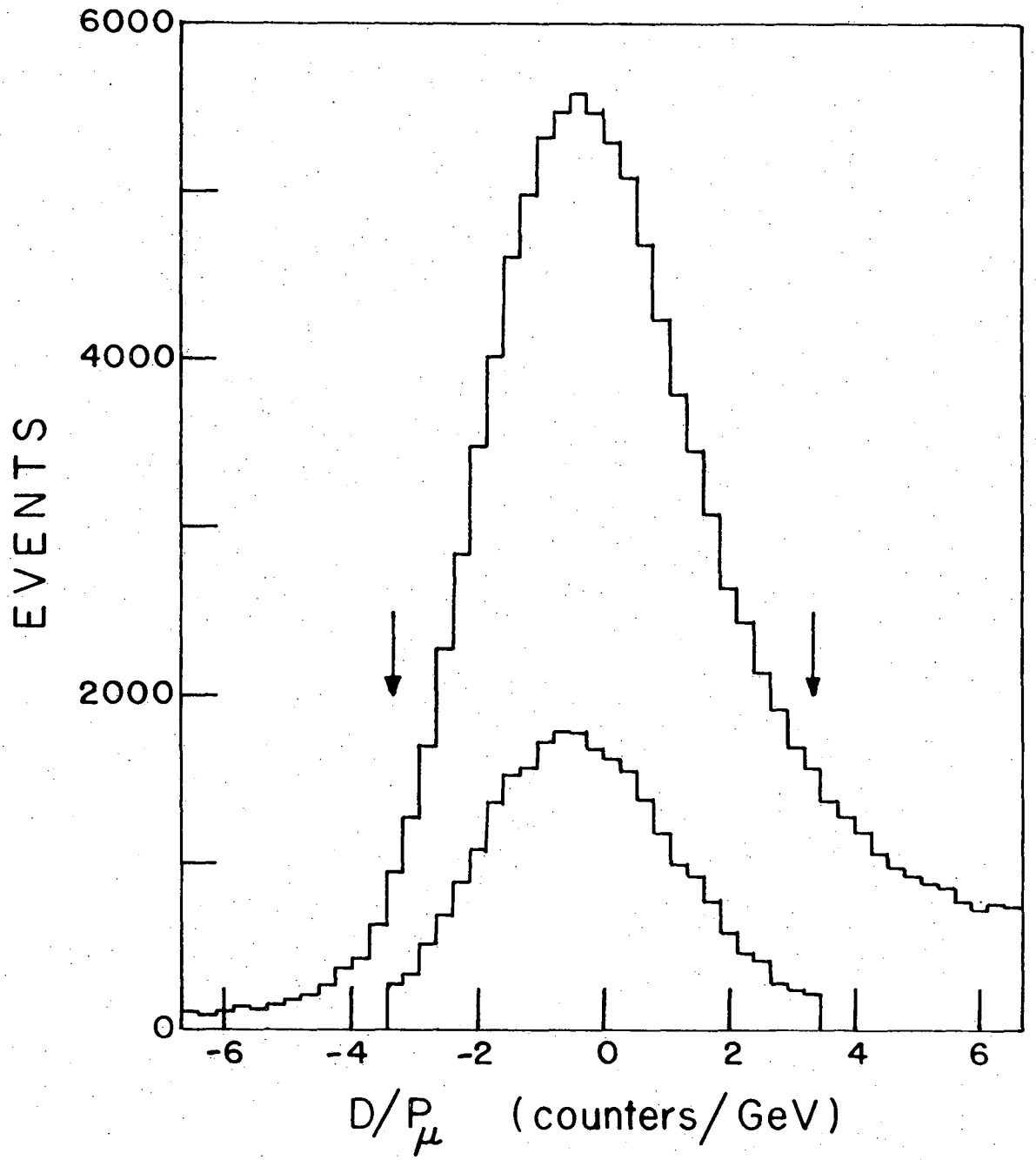

XBL 759-8196

Fig. 7

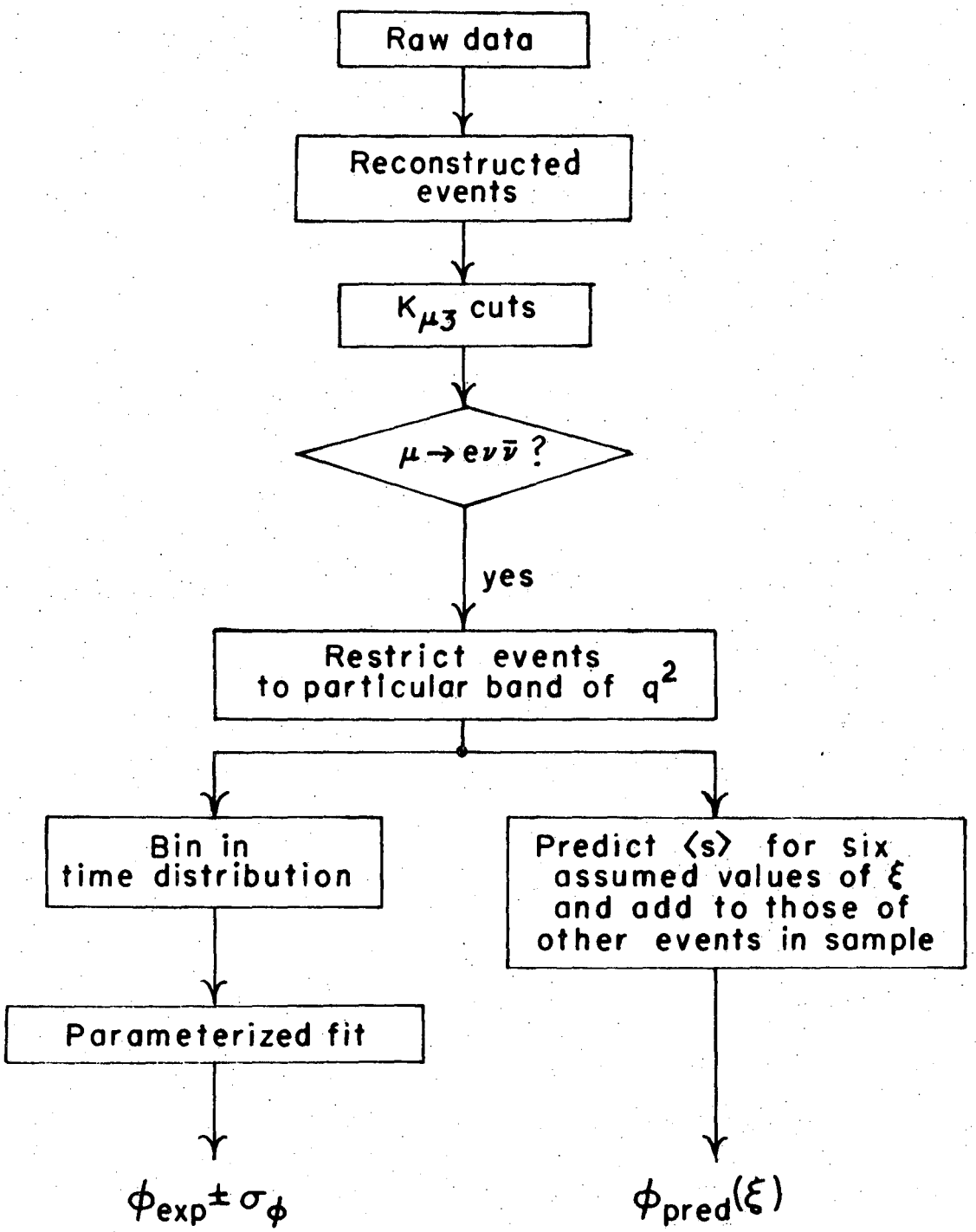

XBL 759-8193

Fig. 8

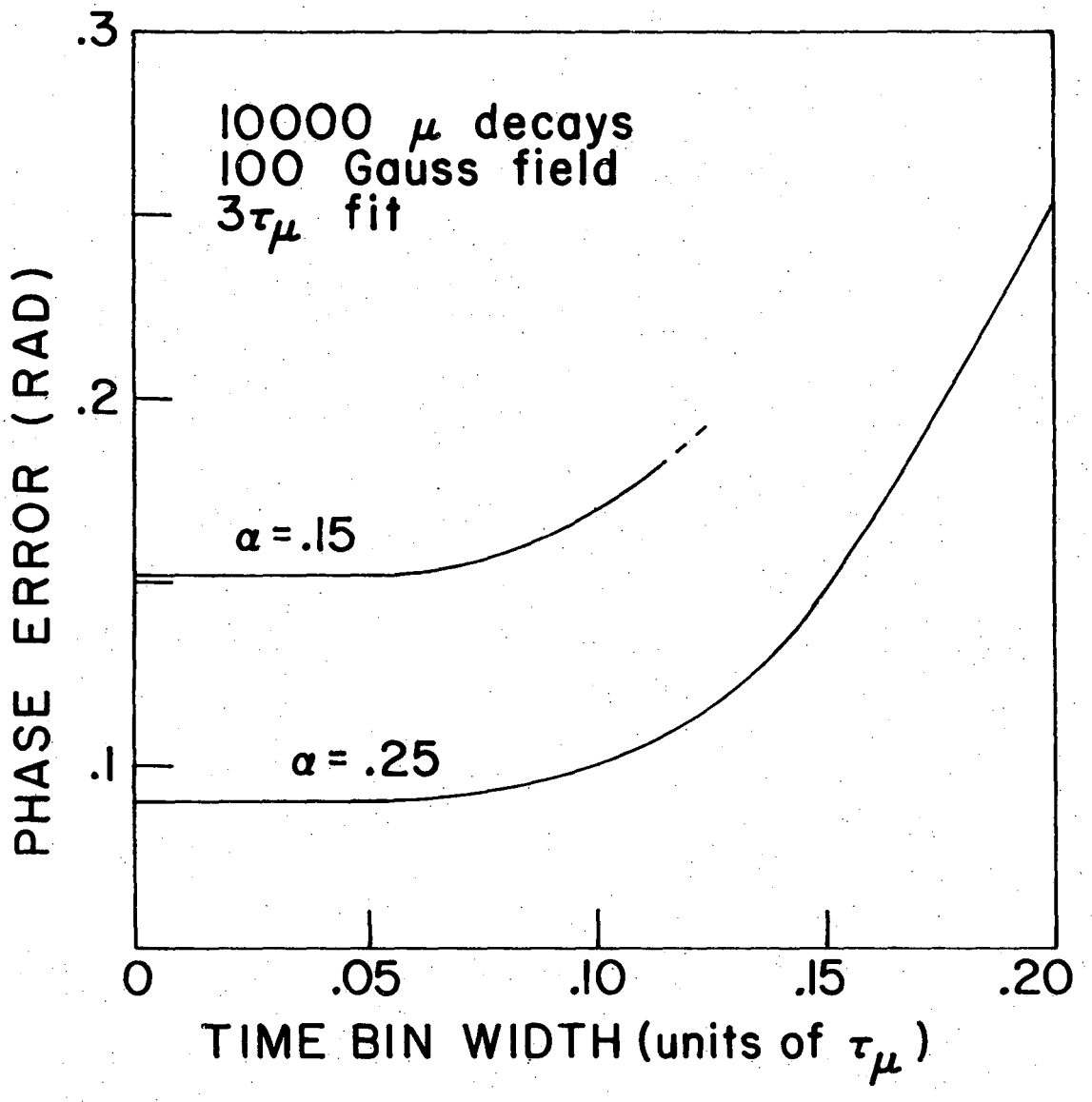

XBL 759-8186

Fig. 9

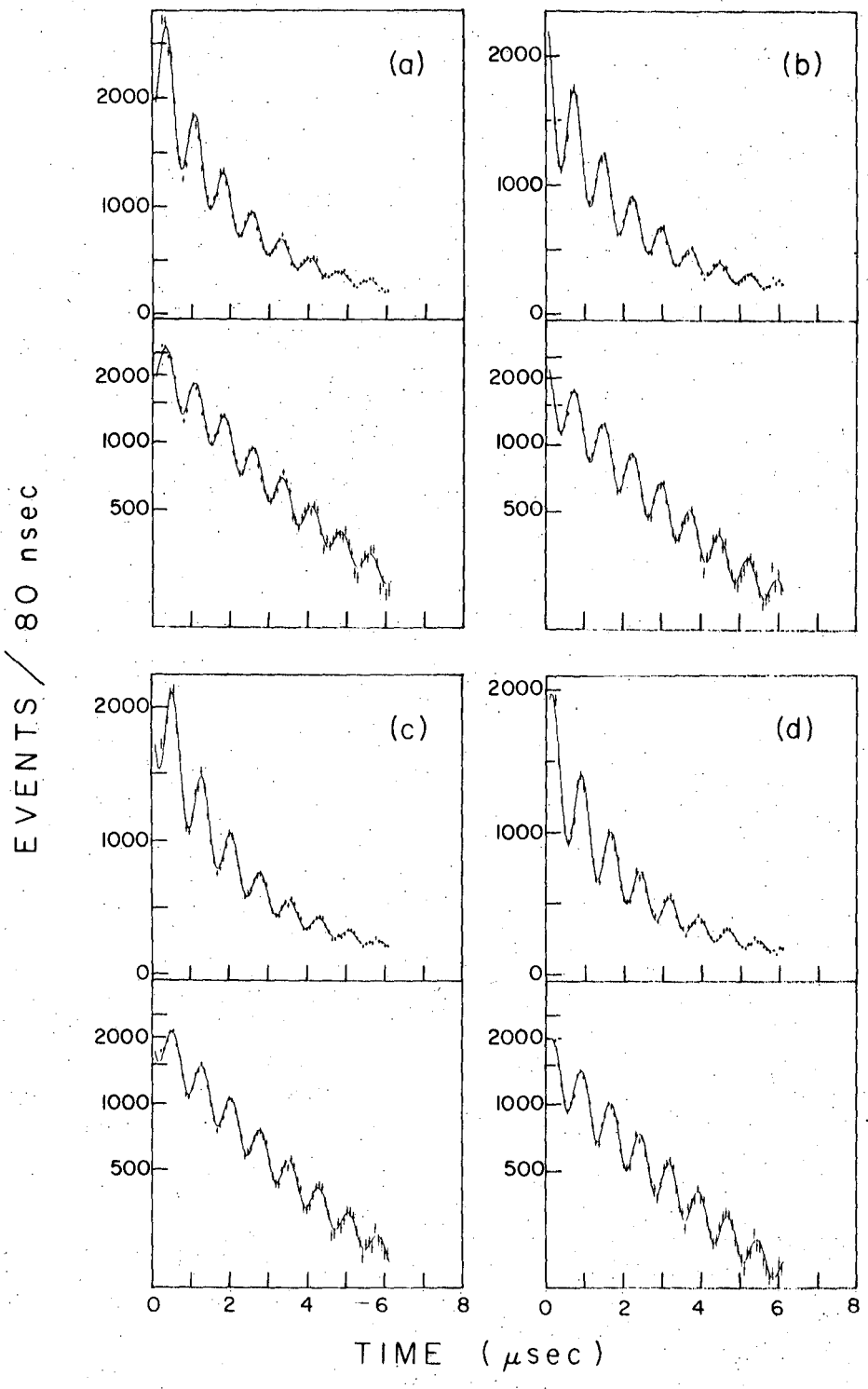

XBL 759-8195

Fig. 10

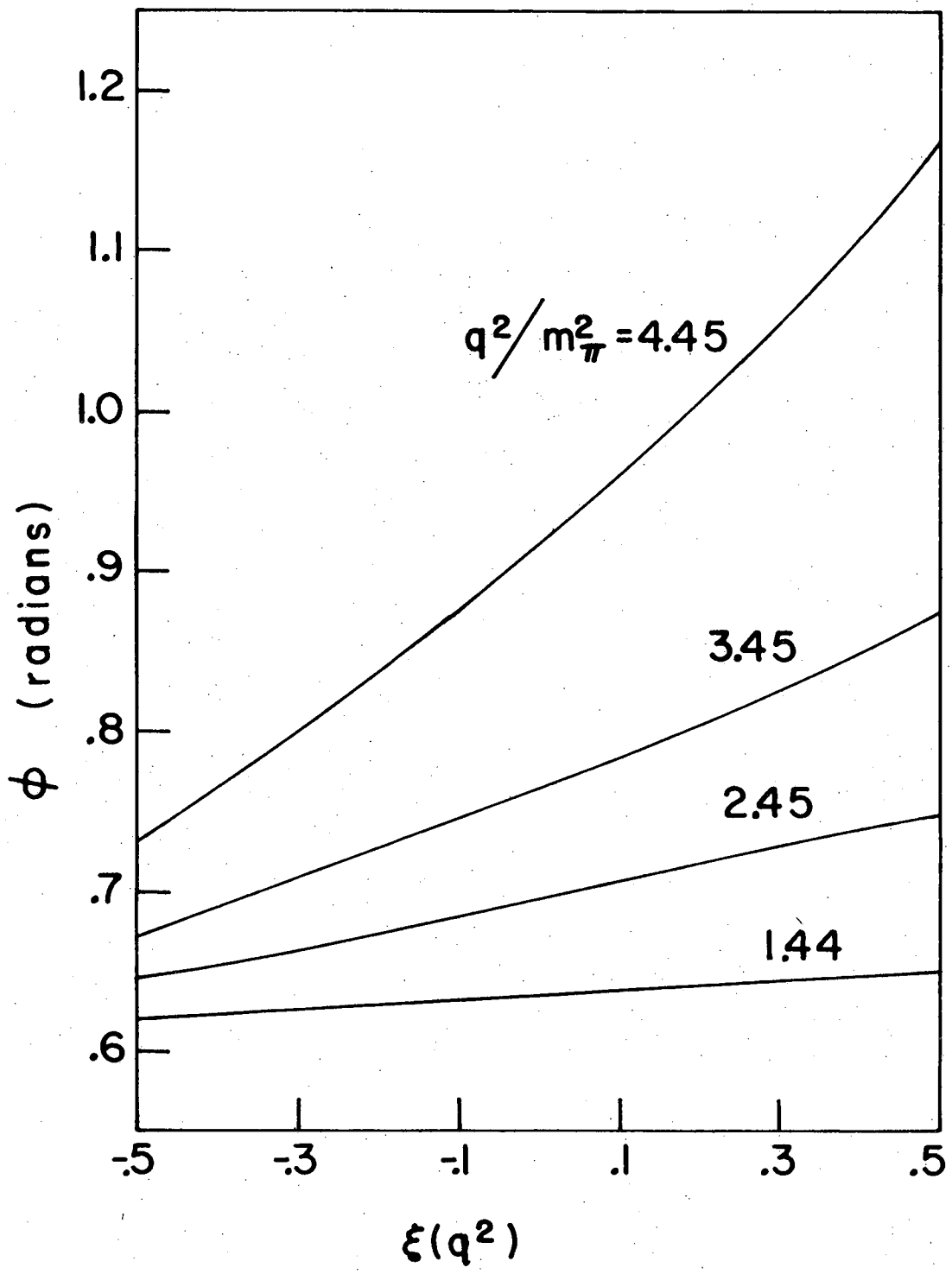

XBL 759-8185A

FIGURE 11

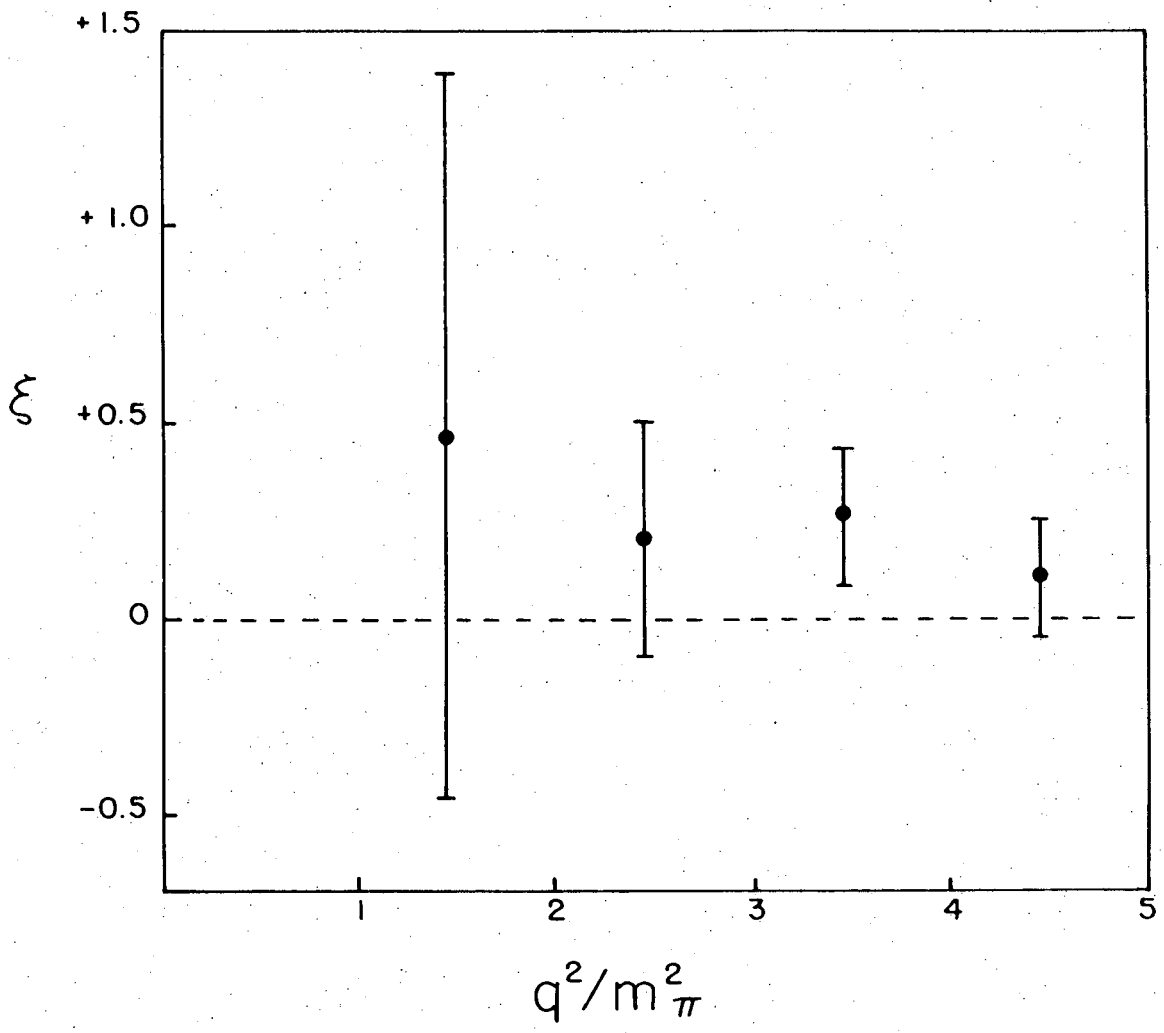

XBL 759-8184

Fig. 12

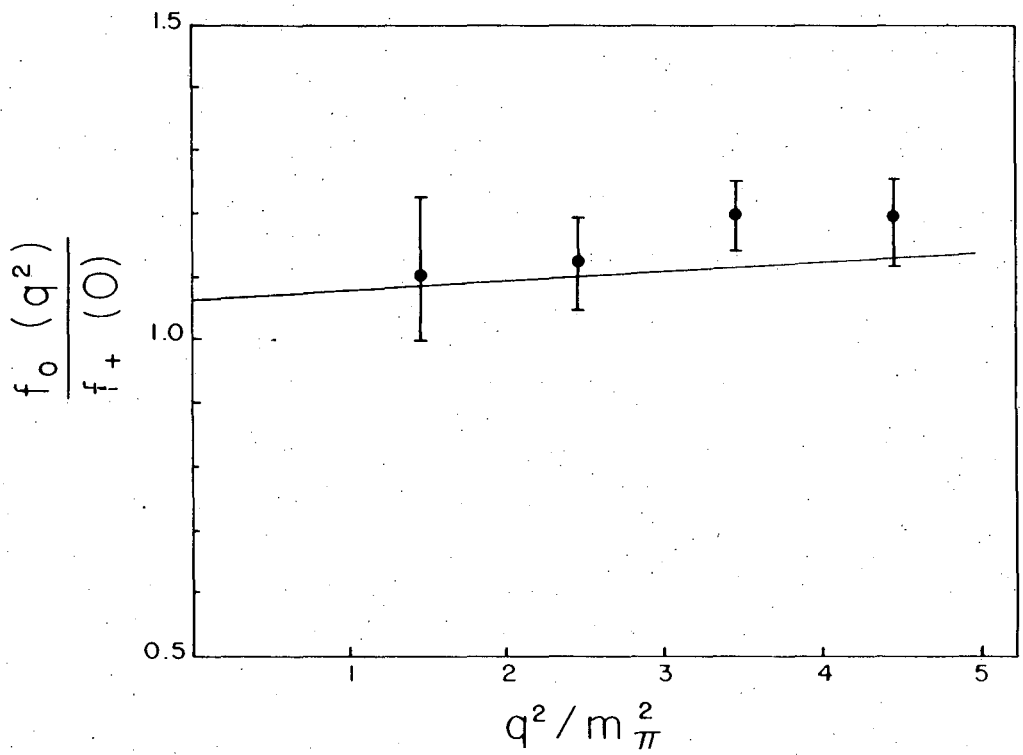

XBL 759 8182

Fig. 13

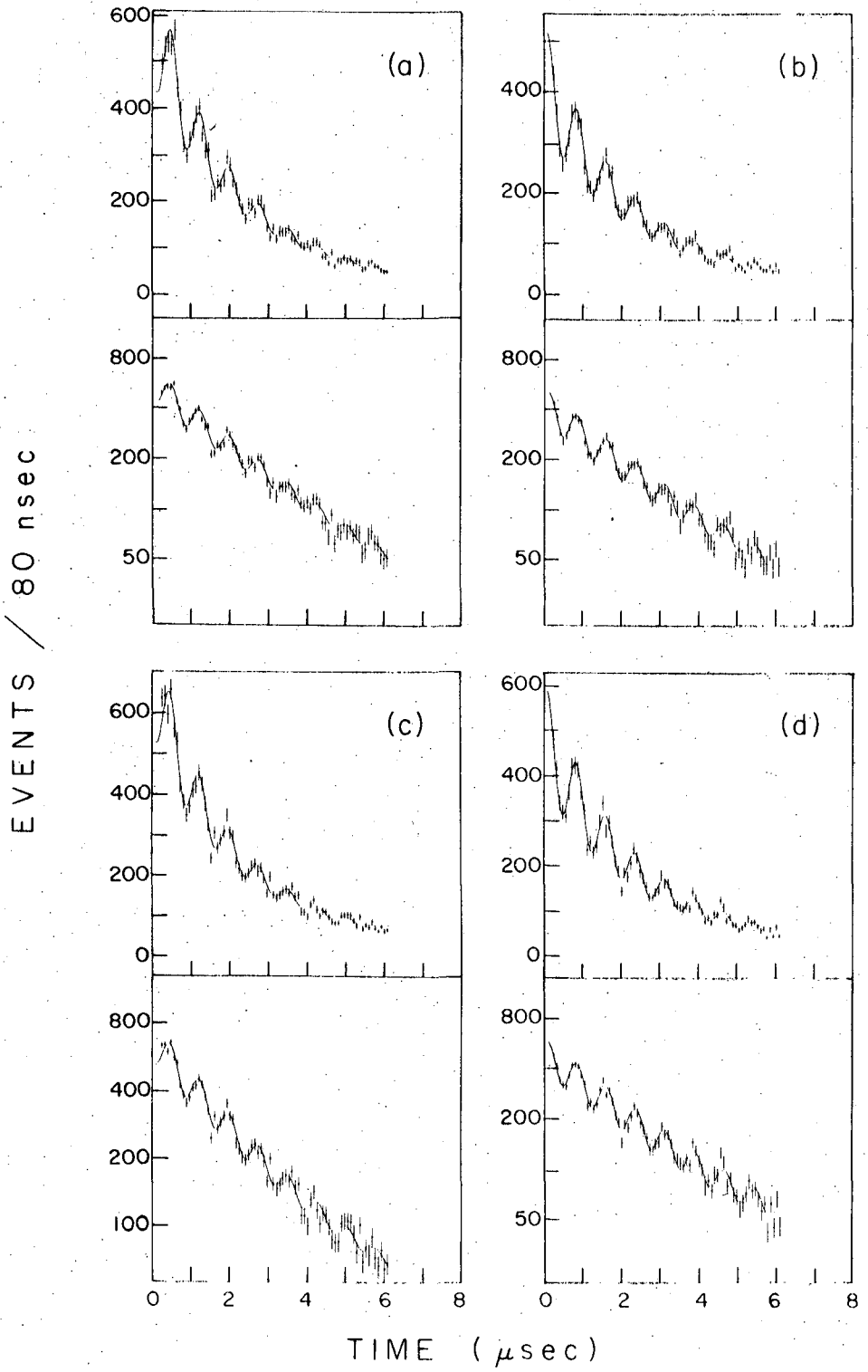

Fig. 14

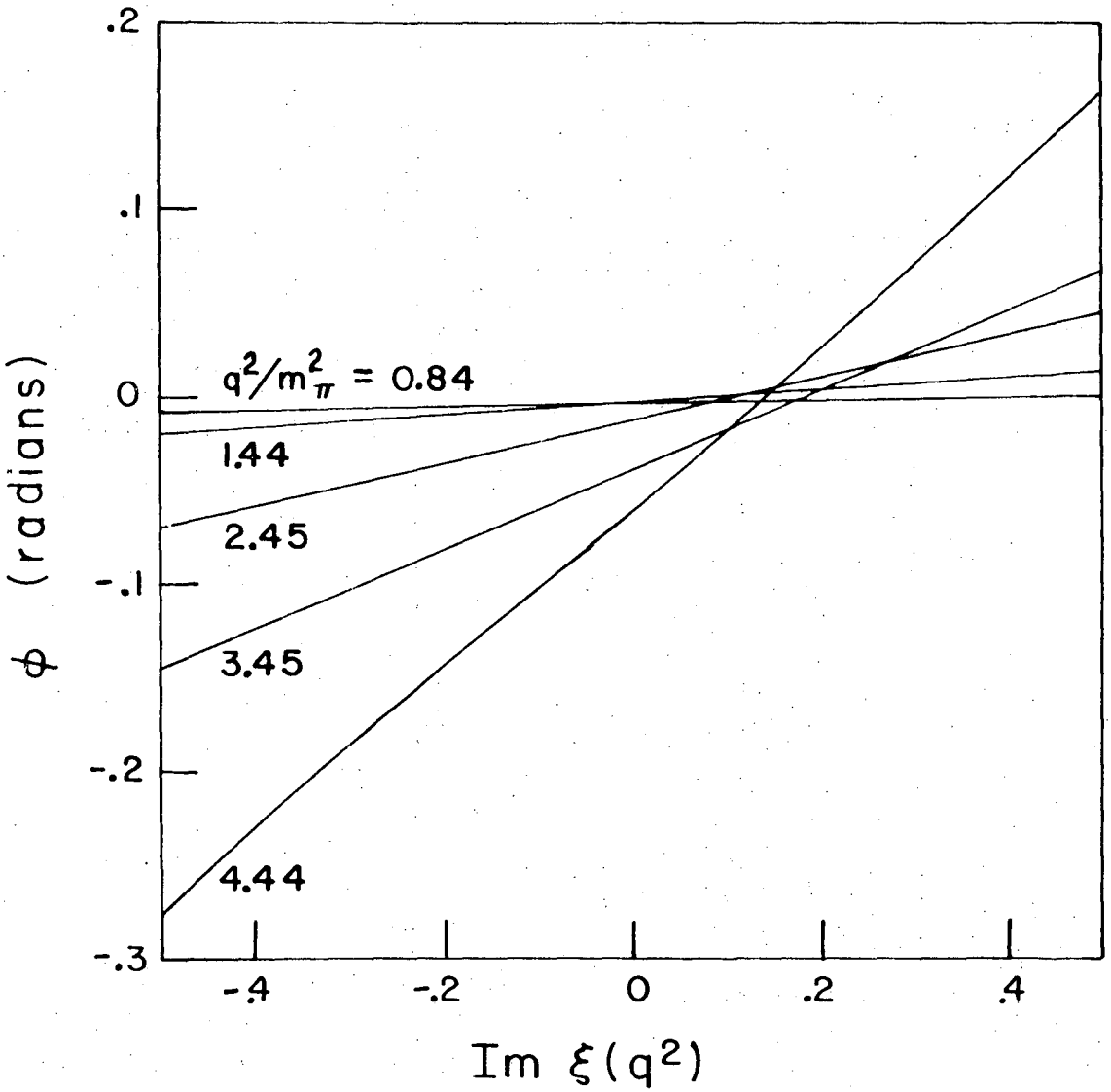

XBL 759-8197

Fig. 15

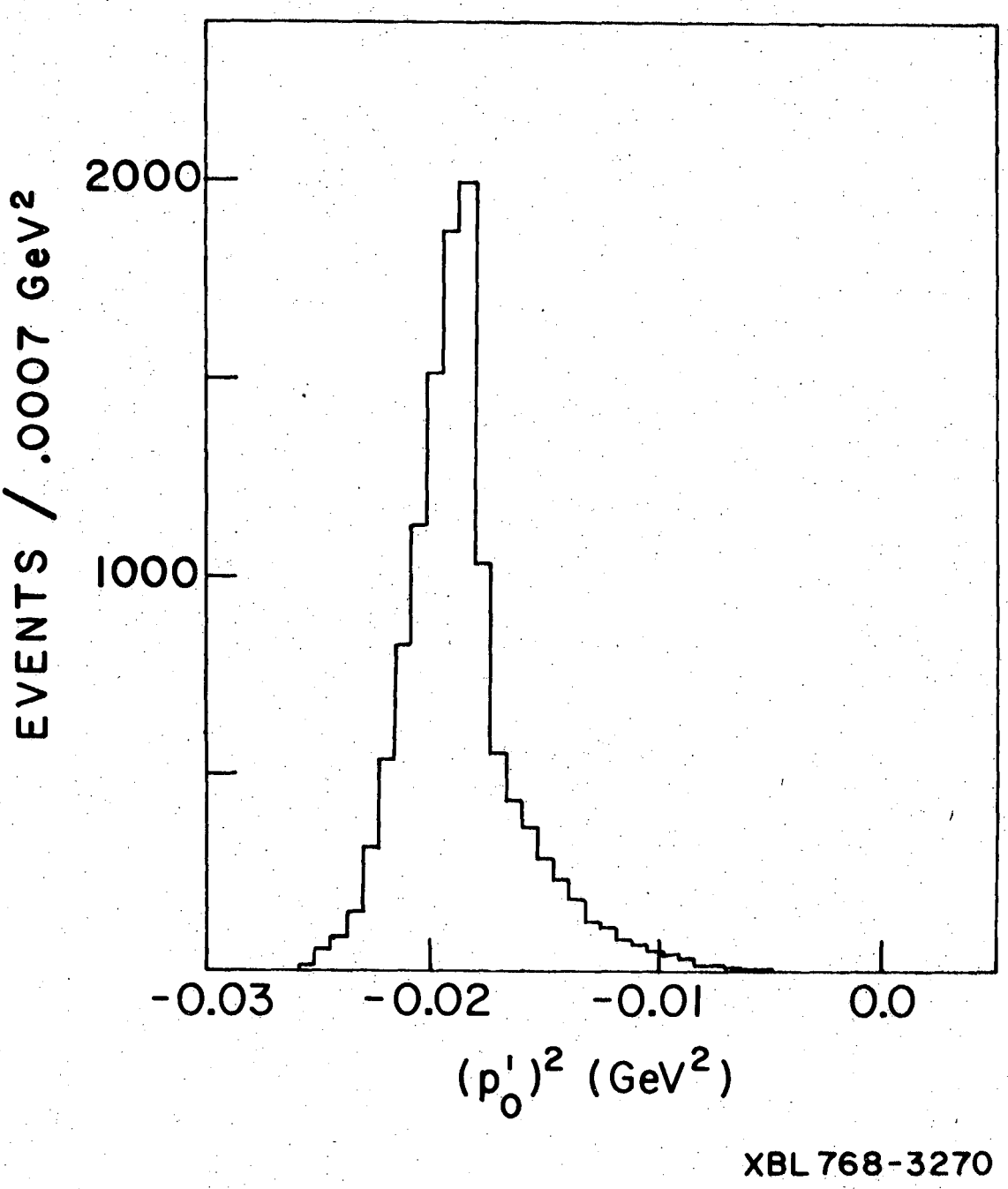

FIGURE 16

This report was done with support from the United States Energy Research and Development Administration. Any conclusions or opinions expressed in this report represent solely those of the author(s) and not necessarily those of The Regents of the University of California, the Lawrence Berkeley Laboratory or the United States Energy Research and Development Administration.

TECHNICAL INFORMATION DIVISION
LAWRENCE BERKELEY LABORATORY
UNIVERSITY OF CALIFORNIA
BERKELEY, CALIFORNIA 94720